Knockdown of a disintegrin A metalloprotease 12 (ADAM12) during adipogenesis reduces cell numbers, delays differentiation, and increases lipid accumulation in 3T3-L1 cells

Chantal A. Coles[a,b,*], Jovana Maksimovic[a,c], Jenny Wadeson[d], Fahri T. Fahri[e], Tracie Webster[d], Carolina Leyton[d], Matthew B. McDonagh[d,f], and Jason D. White[a,b,*]

[a]Murdoch Children's Research Institute, Royal Children's Hospital, Parkville 3052, Australia; [b]Faculty of Veterinary and Agricultural Science and [c]Department of Paediatrics, Faculty of Medicine, Dentistry and Health Sciences, University of Melbourne, Melbourne 3052, Australia; [d]Discovery Technologies, Department of Environment and Primary Industries, Victoria Centre for AgriBioscience, La Trobe University, Melbourne 3083, Australia; [e]Department of Primary Industries, New South Wales Food Authority, Sydney, New South Wales 2001, Australia; [f]Cooperative Animal Research Centre for Sheep Industry Innovation, University of New England, Armidale, New South Wales 2350, Australia

ABSTRACT **Mouse models have shown that a disintegrin A metalloprotease 12 (ADAM12) is implicated during adipogenesis; the molecular pathways are not well understood. Stealth RNA interference was used to knock down ADAM12 in 3T3-L1 cells. Using gene profiling and metabolic enzymatic markers, we have identified signaling pathways ADAM12 impacts upon during proliferation, differentiation, and maturation of adipocytes. ADAM12 reduced cell numbers in proliferating preadipocytes, delayed differentiation of preadipocytes to adipocytes, and increased lipid accumulation in mature adipocytes. The pathway most affected by ADAM12 knockdown was regulation of insulin-like growth factor (IGF) activity by insulin-like growth factor binding proteins (IGFBPs); ADAM12 is known to cleave IGFBP3 and IGFBP5. The IGF/mTOR signaling pathway was down-regulated, supporting a role for ADAM12 in the IGFBP/IGF/mTOR-growth pathway. PPARγ signaling was also down-regulated by ADAM12 knockdown. Gene ontology (GO) analysis revealed that the extracellular matrix was the cellular compartment most impacted. Filtering for matrisome genes, connective tissue growth factor (*Ctgf*) was up-regulated. *CTGF* and IGBP3 can interact with PPARγ to hinder its regulation. Increased expression of these molecules could have influenced PPARγ signaling reducing differentiation and an imbalance of lipids. We believe ADAM12 regulates cell proliferation of preadipocytes through IGFBP/IGF/mTOR signaling and delays differentiation through altered PPAR signaling to cause an imbalance of lipids within mature adipocytes.**

Monitoring Editor
Jonathan Chernoff
Fox Chase Cancer Center

Received: Jul 31, 2017
Revised: May 18, 2018
Accepted: May 23, 2018

INTRODUCTION

A disintegrin A metalloprotease 12 (ADAM12) belongs to the metzincin family of proteases characterized by a highly conserved motif of three histidines that bind zinc at the catalytic domain and conserved methionine residue (Sternlicht and Werb, 2001). ADAM12 has the following domains: a signal peptide, propeptide, metalloprotease, disintegrin, cysteine-rich region, epidermal

This article was published online ahead of print in MBoC in Press (http://www.molbiolcell.org/cgi/doi/10.1091/mbc.E17-07-0471) on May 30, 2018.

The authors have no conflicts of interest to declare.

*Address correspondence to: Chantal A. Coles (chantal.coles@mcri.edu.au) or Jason D. White (jasondw@unimelb.edu.au).

Abbreviations used: ADAM12, a disintegrin and metalloprotease 12; AMPK, adenosine monophosphate–activated protein kinase; CTGF, connective tissue growth factor; DE, differentially expressed; ECM, extracellular matrix; FAS, fatty acid synthase; G3PDH, glycerol-3-phosphate dehydrogenase; GO, gene ontology; IGF, insulin-like growth factor; IGFBP, insulin-like growth factor binding proteins; MNE, mean normalized gene expression; mTOR, mechanistic target of rapamycin; PPARγ, peroxisome proliferator-activated receptor gamma; RNAi, RNA interference.

growth factor (EGF) -like repeat, transmembrane, and cytoplasmic tail (Duffy *et al.*, 2003). A conserved site of the prodomain, named the cys residue, coordinates the active zinc site to inhibit catalysis resulting in the protease to remain as a zymogen, known as the cysteine-switch mechanism (Loechel *et al.*, 1998; Streuli, 1999; Page-McCaw *et al.*, 2007). Metalloprotease catalysis is dependent on removal of the prodomain by instability of the cysteine switch to expose the active zinc site to enable cleavage of substrates (Loechel *et al.*, 1998). The disintegrin domain and cysteine-rich region are also involved in cell–cell interactions. The disintegrin domain binds integrins and the cysteine-rich region supports syndecan-mediated cell adhesion (Schlondorff and Blobel, 1999; Zolkiewska, 1999; Eto *et al.*, 2000; Iba *et al.*, 2000). There are two splice variants of ADAM12, referred to as the long transmembrane form, ADAM12-L, and the short soluble secreted form, ADAM12-S. ADAM12-S has all the extracellular domains of ADAM12-L but lacks the transmembrane domain and cytoplasmic tail; instead, the EGF-like repeat is followed by a unique 33 amino acid sequence. Unlike the transmembrane-bound long form ADAM12-L, ADAM12-S is secreted in the extracellular matrix and detected in serum and urine (Wewer *et al.*, 2006).

ADAM12 is expressed by adipocytes during adipogenesis (Kawaguchi *et al.*, 2002, 2003; Kurisaki *et al.*, 2003; Masaki *et al.*, 2005). Intra- and extracellular roles for ADAM12 during adipogenesis in vitro have been proposed: 1) reorganizing the actin cytoskeleton when flat preadipocytes round up, in preparation to lipid-fill into mature adipocytes (Kawaguchi *et al.*, 2003); and 2) to reorganize the fibronectin-rich extracellular matrix, a crucial step in adipogenic differentiation (Kawaguchi *et al.*, 2003). ADAM12 gene knockout mice and transgenic mice overexpressing ADAM12 demonstrate a role for ADAM12 during adipogenesis. Mice overexpressing ADAM12-S and ADAM12-L showed an accumulation of adipocytes within striated skeletal muscle of the abdominal wall, hind limb, and diaphragm indicative of increased adipogenesis (Kawaguchi *et al.*, 2002). Adipocytes in ADAM12-L –overexpressing mice were not as abundant within skeletal muscle when compared with mice overexpressing ADAM12-S (Kawaguchi *et al.*, 2002). ADAM12-S mice lacking the pro- and metalloprotease domain did not display enhanced adipogenesis, suggesting the catalytic metalloprotease domain is crucial for adipogenesis. PPARγ, the master regulator of adipogenesis, was also found to be up-regulated in developing adipocytes found within connective tissue of skeletal muscle in close proximity to blood vessels of mice overexpressing ADAM12 (Kawaguchi *et al.*, 2002). This suggests ADAM12 is involved in the development of adipocytes that originate from mesenchymal progenitor or preadipocytes within the perivascular space of connective tissue (Kawaguchi *et al.*, 2002).

ADAM12 gene knockout mice display a significant reduction in the interscapular brown adipose tissue (BAT) and a mild skeletal muscle defect in the neck and interscapular muscles (Kurisaki *et al.*, 2003). HB-EGF (a substrate of ADAM12) ectodomain shedding was also reduced in ADAM12–deficient mice (Kurisaki *et al.*, 2003). A study by Masaki *et al.* (2005) found ADAM12 knockout mice were resistant to obesity induced by a high-fat diet, due to a reduced ability of adipocytes to proliferate. HB-EGF was involved in this phenotype but rather inhibited adipogenesis, questioning a role for ADAM12 ectodomain sheddase activity in promoting adipogenesis as suggested by Kurisaki *et al.* (2003). Another substrate of ADAM12, IGFBP-3 is thought to contribute to IGF-I–dependent proliferation during adipogenesis (Masaki *et al.*, 2005). This is thought to induce proliferation through ADAM12 cleavage of IGFBP-3 to make IGF-I available to activate IGF-I receptor (Shi *et al.*, 2000).

ADAM12 has shown that it is an important regulator of fat development. However, the exact role ADAM12 has during adipocyte proliferation and differentiation is still unclear. This investigation aims to determine the molecular pathways ADAM12 influences during proliferation and differentiation of adipocytes. We have used Stealth RNA interference (RNAi) to knock down ADAM12, and gene profiling in an in vitro murine fat development model to determine the signaling pathways ADAM12 regulates during adipogenesis.

RESULTS

ADAM12 gene knockdown reduced cell numbers and affected differentiation and mature adipocyte development

Phase images demonstrate the morphological change during adipocyte differentiation from flattened preadipocytes (day 6) to mature lipid-filled adipocytes (day 9–day 13; Figure 1). Cell numbers (DNA [μg/ml]) were reduced in ADAM12 RNAi cells for day 3 (control: 5.315 μg/ml; ADAM12 RNAi: 4.731 μg/ml), day 6 (control: 9.426 μg/ml; ADAM12 RNAi: 8.003 μg/ml), and day 9 (control: 6.704 μg/ml; ADAM12 RNAi: 5.207 μg/ml; REML treatment effect, $p < 0.05$; Figure 1, Day 6, and Figure 2A). Concentration of DNA (μg/ml) peaked on day 6 for control and ADAM12 RNAi (Figure 2A). These results suggest that ADAM12 gene knockdown reduced cell numbers in 3T3-L1 cells. ADAM12 RNAi delayed the rate at which preadipocytes rounded up to form adipocytes (Figure 1). The proportion of preadipocytes to adipocytes differed between ADAM12 RNAi and control cells. On day 9, ADAM12 RNAi–treated cells had a higher proportion of preadipocytes to adipocytes compared with the control (ADAM12 RNAi preadipocytes 55.64%: adipocytes 44.36%; control preadipocytes 20.36%: adipocytes 79.64% [*t* test, $p < 0.01$]); refer to Figure 2B. Cell size of adipocytes was also found to be different between ADAM12 RNAi and control. On days 9 and 13 the mean diameter of adipocytes was not found to be different between ADAM12 RNAi (29.4 μm)-treated cells and the control (27.6 μm; Figure 2C). The diameter of lipids with one, two, or three droplets was measured in control and ADAM12 RNAi adipocytes. The mean diameter of lipid droplets contained within mature adipocytes was found to be different between the control and ADAM12 RNAi cells. On day 9, adipocytes with two lipid droplets (*t* test, $p < 0.01$) were found to be smaller in ADAM12 RNAi cells compared with control cells (control: one droplet, 8.24 μm; two droplets, 7.73 μm; three droplets, 7.14 μm vs. ADAM12 RNAi: one droplet, 6.10 μm; two droplets, 4.84 μm; three droplets, 5.49 μm); see Figure 2D. However, on day 13, lipids containing one (*t* test, $p < 0.01$) and three (*t* test, $p < 0.05$) droplets were found to be larger in ADAM12 RNAi (control: one droplet, 4.16 μm; two droplets, 4.79 μm; three droplets, 6.84 μm vs. ADAM12 RNAi: one droplet, 11.52 μm; two droplets, 7.61 μm; three droplets, 9.66 μm); refer to Figure 2D. These findings suggest ADAM12 is involved in differentiation of fibroblastic-like preadipocytes into round adipocytes and development of mature lipid-filled adipocytes. To rule out the possibility that increased apoptosis was driving this effect, we evaluated the expression of *Bcl2* and *Bax*, two key regulators of apoptosis. At the early stages of ADAM12 knockdown (day 3), expression of *Bcl2* transcript was increased; there was no difference compared with controls at days 6 and 9. At no stage was the expression of *Bax* affected by inhibition of ADAM12 expression.

ADAM12 gene knockdown affected enzymatic markers of lipogenesis

G3PDH (glycerol-3-phosphate dehydrogenase) enzyme activity was used as an early marker of adipocyte differentiation in response to ADAM12 gene knockdown. Its activity is correlated to the early stages of glucose metabolism (lipogenesis) during adipogenesis.

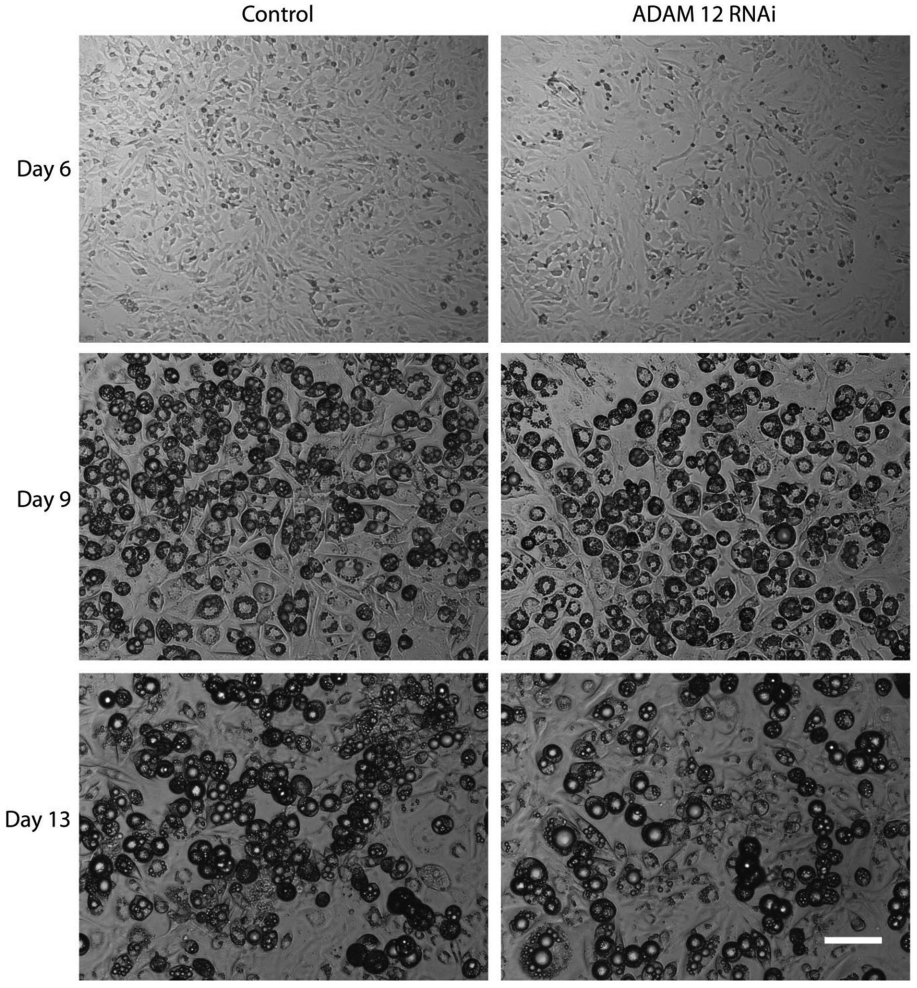

FIGURE 1: 3T3-L1 cells at day 6, day 9, and day 13 in control and ADAM12 RNAi–treated adipocytes. Cell numbers are reduced at day 6 in ADAM RNAi. Fewer preadipocytes and differentiated cells are evident in ADAM12 RNAi cells, particularly at day 6. Larger lipid droplets are seen in ADAM12 RNAi–treated cells compared with RNAi control on day 13. Scale bar represents 100 μm.

G3PDH activity was found to be different between ADAM12 RNAi and control cells for day 9, day 12, and day 15 (REML treatment effect, $p < 0.05$; refer to Figure 3A). The effect of ADAM12 knockdown on fatty-acid synthesis during latter stages of adipogenesis was assayed by measuring fatty-acid synthase (FAS) activity. This relates to lipid filling (triglyceride anabolism) in maturing adipocytes. FAS activity (nmol of NADH oxidized by FAS per minute per microgram of DNA) was increased in ADAM12 RNAi compared with control on day 9 (*t* test, $p < 0.05$); see Figure 3B. These results, supported by an increase in the size of lipid droplets at day 13 (Figure 2), suggests there was increased lipogenesis in ADAM12 RNAi cells during stages where adipocytes were lipid-filling.

Gene profiling

Quality control and ADAM12 gene knockdown. Multidimensional scaling analysis of the filtered and normalized microarray data showed that time was the biggest factor influencing the data, with day 3 (T3), day 6 (T6), and day 9 (T9) samples all showing separation in the first principal component (Figure 4A). A control sample at T3 and ADAM12 RNAi sample at T9 were outliers from their respective groups in the second principal component; however, they did cluster with their corresponding time points in the first principal component (Figure 4A). With the outlying samples removed, the remaining samples cluster tightly within their time points in the first two principal components (Figure 4B). Clear separation between treatment groups (control and ADAM12 RNAi) can be seen in the fourth principal component, with the outliers (T3 and T9) removed (Figure 4C). Box plots of ADAM12 gene expression show that its expression is reduced in ADAM12 RNAi cells compared with control (Figure 5A), although the knockdown effect did diminish over time, with little difference in expression observed at T9.

Differentially expressed gene. T3 showed the highest number of significantly differentially expressed (DE) genes at false discovery rate (FDR) < 0.05 (T3 DE Total: 2508, UP: 1397, DOWN: 1111; Figure 5, B and C). At T6, as the cells differentiated and the magnitude of the gene knockdown diminished, the number of DE genes was reduced (T6 DE total: 1090; UP: 569; DOWN: 521). A further reduction in the number of DE genes was evident at T9 (T9 DE Total: 623; UP: 366; DOWN: 257). Although ADAM12 gene expression returned to control levels in T9, substantial differences are still evident at T9, both at the transcript level and at the protein level, based on the phenotype observed in vitro. We believe that these differences are attributed to changes occurring early in the time course when cells are proliferating and differentiating; in particular, changes in the extracellular matrix which are crucial for adipogenesis. A Venn diagram of the DE genes at each time point shows the greatest overlap between the DE genes at T3 and T6 (308 genes), followed by T6 and T9 (137 genes), then T3 and T9 (92 genes; Figure 5C). We also identified a set of genes that were significantly differentially expressed between control and ADAM12 RNAi cells across all three time points (T3, T6, and T9), irrespective of ADAM12 gene expression returning at T9. We have named this gene set "ALL." The number of DE genes in the ALL gene list was 1152. Gene lists for DE genes for each time comparison can be found in Supplemental File 1. Heatmaps of the expression levels of the top DE genes for each comparison (FDR < 0.05 and |FC| > 2) highlight the differences in gene expression between ADAM12 RNAi and control samples, as well as the changes over time due to the diminishing effect of the knockdown (Figure 6). The samples generally cluster both by time point and treatment, for all comparisons. For the ALL comparison, the difference between the ADAM12 RNAi and control is obvious at all three time points; however, the overall level expression for many of the genes does tend to change substantially over time (Figure 6A). For the comparisons at individual time points, as expected, the difference beween treatment and control is most apparent at the time point tested, and tends to be less visible at the other time points (Figure 6, B–D). This is most striking for the genes found to be DE at T3 where the samples fail to cluster based on ADAM12 RNAi treatment by T9 (Figure 6B). This indicates that these are likely to be the genes most directly impacted by the ADAM12 knockdown.

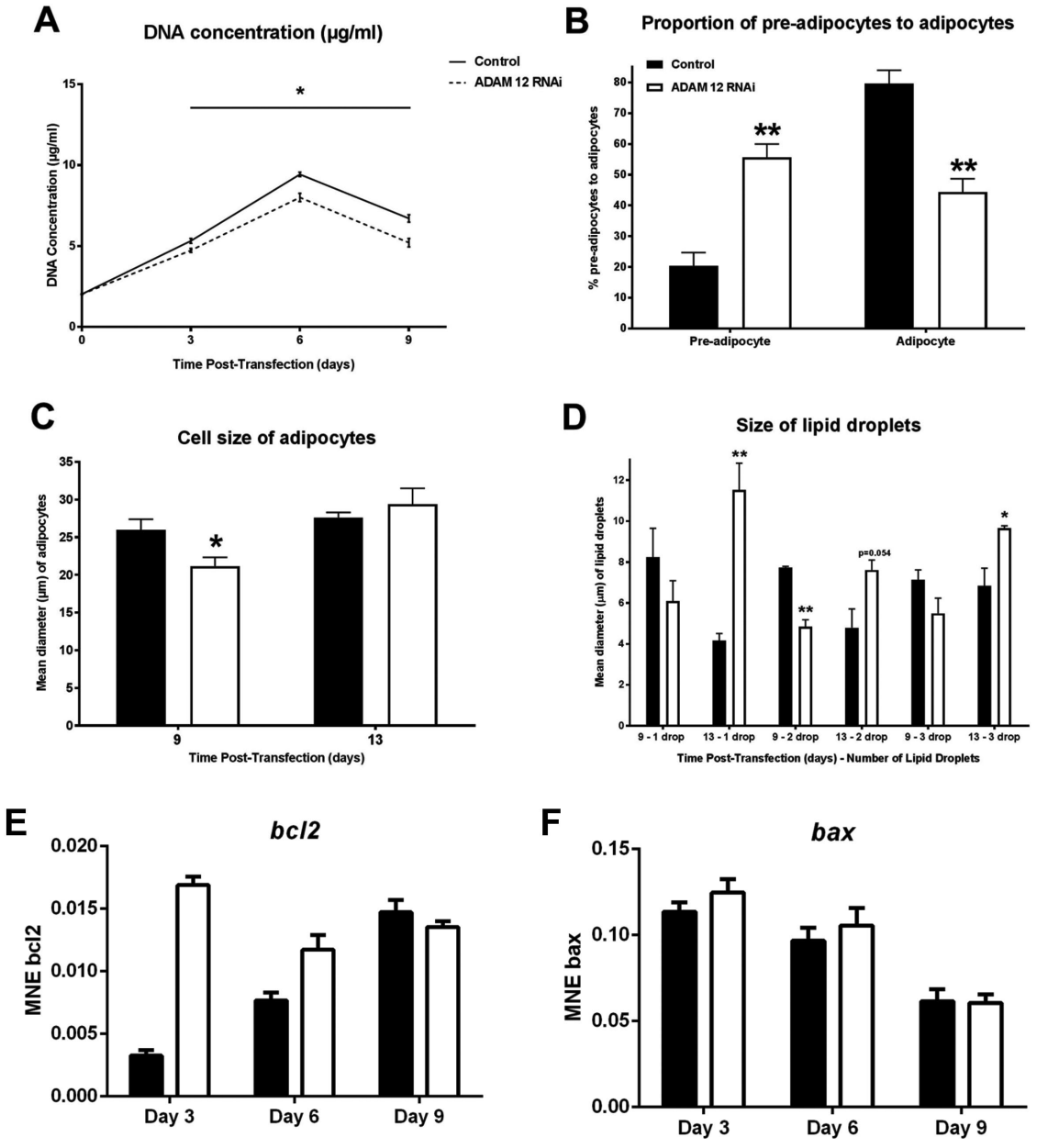

FIGURE 2: Effect of ADAM12 knockdown on cell numbers, morphology, and lipid accumulation in mature 3T3-L1 adipocytes. (A) Cell numbers were reduced in ADAM12 RNAi cells (DNA [µg/ml]). (B) Proportion of preadipocytes to adipocytes on day 9 posttransfection was increased in ADAM12 RNAi cells suggesting differentiation was delayed. (C) Cell size (in diameter [µm]) of adipocytes was reduced in ADAM12 RNAi cells. (D) Size of lipid droplets (in diameter [µm]) in mature adipocytes that contain either one droplet, two droplets, or three droplets of lipid on day 9 and day 13 were measured. (E) Size of lipid droplets were increased on day 13 in ADAM12 RNAi cells. Expression of *Bcl2* was up-regulated in ADAM12 RNAi cells at day 3 but was not changed at days 6 or 9. (F) The expression of *Bax* was not affected by inhibition of ADAM12 expression. *, $p < 0.05$; **, $p < 0.01$ ($n = 3$ for control and ADAM12 RNAi at each time point).

Gene ontology analysis. Gene ontology (GO) analysis on the DE genes for each comparison—T3, T6, T9 and ALL—showed that ADAM12 appears to be impacting the extracellular matrix (ECM). The top 10 GO terms for each comparison can be seen in Figure 7. For the ALL (Figure 7A), T6 (Figure 7C), and T9 (Figure 7D) comparisons, at least 4 of the top 10 GO terms were related to the ECM. At T3 (Figure 7B), the top GO terms were predominantly associated with immune function/response, with only one GO term linked to the ECM. Refer to Supplemental File 2 for a full list of GO terms impacted by ADAM12 knockdown for ALL, T3, T6, and T9.

DE matrisome genes. From the GO analysis we established that the effects of ADAM12 gene knockdown were predominantly impacting the ECM. We then wanted to determine what genes were involved in causing these changes. Using the DE gene lists ALL, T3, T6, and T9, we filtered these genes against a list of known core-matrisome proteins (Naba *et al*. 2012); this includes a total of 274 genes (43 collagens, 36 proteoglycans, and 195 glycoproteins). Table 1 outlines the top 10 core-matrisome proteins differentially expressed (top five up-regulated and five down-regulated) with knockdown of ADAM12; refer to Supplemental File 3 for an extensive list. The total number of core-matrisome genes differentially

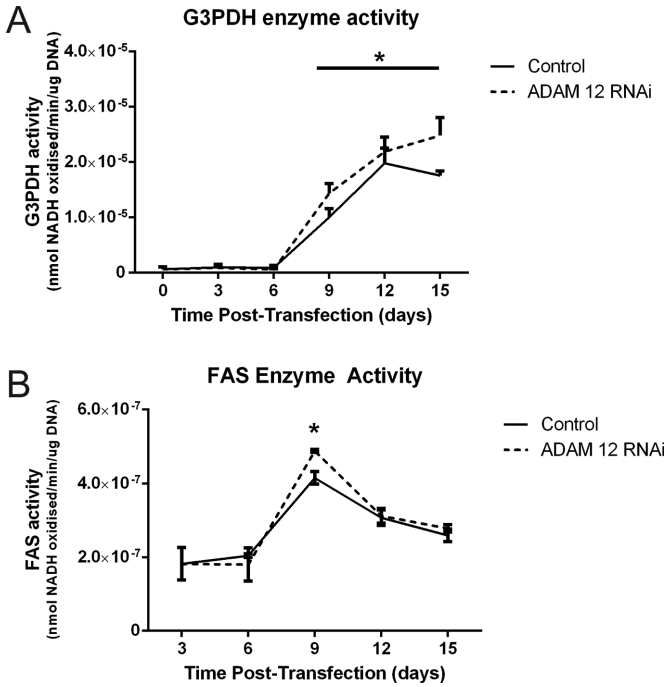

FIGURE 3: (A) Enzymatic markers of differentiation/lipogenesis are increased in ADAM12 RNAi cells. Enzyme activity of glycerol-3-phosphate dehydrogenase (G3PDH; nmol NADH oxidized per min/μg DNA) and (B) enzyme activity of fatty-acid synthase (FAS; nmol NADH oxidized per min/μg DNA) in 3T3-L1 cell lysates from ADAM12 RNAi and control cells. *, $p < 0.05$ ($n = 3$ for control and ADAM12 RNAi at each time point).

expressed in ADAM12 RNAi cells was 62 for ALL comparison, 58 for T3, 57 for T6, and 48 for T9. *Ctgf* (connective tissue growth factor) was the most highly up-regulated matrisome gene for ALL (1.08-fold), T3 (2.37-fold) and T6 (1.20-fold) followed by *Mfap5* (microfibrillar-associated protein 5) at time points ALL (1.03-fold), T3 (1.23-fold), and T6 (1.02-fold). Validation by qRT-PCR found *Ctgf* to be up-regulated at T2 and T3 ($p < 0.05$). Collagens are important structural ECM proteins fundamental to support the dramatic morphological changes in the adipocytes during differentiation. Proteins associated with collagen binding and synthesis were also found to be the greatest up-regulated core-matrisome genes; these included *Dcn* (decorin; ALL, 0.87-fold), *Lum* (lumican; T6, 0.93), *Fbn1* (fibrillin 1; ALL, 0.94-fold), and *Fbln7* (fibulin 7; ALL, 0.84-fold; T9, 1.39-fold). In light of these collagen -associated proteins being up-regulated, a number of collagen isoforms were found to be the most down-regulated matrisome genes. These included *Col5a3* (ALL), *Col5a2*, *Col4a5*, *Col11a1* (T3), and *Col5a3*, *Cola4a2*, *Col6a3* (T6). In addition, *Lama5* (laminin α5; ALL, T6) and *Lamb3* (laminin β3; T9) was also one of the most down-regulated core-matrisome genes. Validation by qRT-PCR found *Fbn1* (see Figure 10D later in the paper) to be up-regulated at T2, T3, and T6 (REML treatment effect, $p < 0.05$), *Col6a3* (see Figure 10J later in the paper) down-regulated at T2, T3, T6, and T9 (REML treatment effect, $p < 0.05$), and *Lum* (10I) to be up-regulated at T6 ($p < 0.05$).

In addition to core-matrisome proteins, we were also interested in proteins associated with the matrisome, such as cytokines, chemokines, growth factors, mucins, galectins, plexins, serine proteases, matrix metalloproteases, and other ECM-associated proteins. Using a list of all 619 matrisome genes from the Broad Institute Molecular Signatures Database (MSigDB) curated (C2) set, which includes 177 core-matrisome and 444 matrisome-associated proteins, we found 203 DE genes for T3, 158 for T6, and 142 for T9. Out of these DE genes, 36 were consistently different across all time points (T3, T6, and T9), 41 genes overlap between T3 and T6, 39 between T6 and T9, and 20 between T3 and T9; refer to Figure 8. A summary of the 20 top-ranked genes (FDR < 0.05) is presented in Figure 8 for all comparisons, showing most matrisome genes are up-regulated. MMP3 was in the 20 top-ranked genes for all comparisons. *Mfab5* and *Fbn1* were in the top ranked for ALL, T6, and T9, and *Ctgf* was top ranked for T3 and T6. The full list of DE matrisome genes in ADAM12 knockdown cells for each comparison can be found in Supplemental File 4.

Pathway analysis. To determine which pathways were affected in ADAM12 RNAi cells, we performed gene set testing of all the canonical pathways from the MSigDB C2 set. The top 10 canonical pathways for the ALL comparison and the six top-ranked sets for T3, T6, and T9 comparisons are summarized in Table 2; refer to Supplemental File 5 for the full lists. Regulation of IGF activity by IGFBPs was the top-ranked pathway for the ALL comparison; ADAM12 is known to cleave IGFBP3 and IGFBP5 (Loechel *et al.*, 2000; Shi *et al.*, 2000). The same pathway was ranked second at T6 and was also the

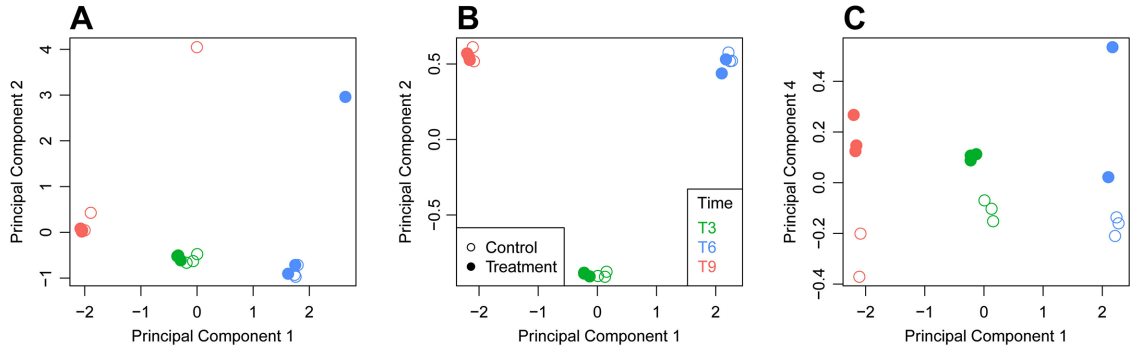

FIGURE 4: Quality control for microarray gene profiling. Principal component analysis (PC) for the gene expression of control and ADAM12 RNAi–treated (treatment) adipocytes at each time point (T3: day 3 posttransfection; T6: day 6 posttransfection; T9: day 9 posttransfection). (A) PC1 vs. PC2 shows the greatest effect is time. Two outliers are evident for T3 and T9. (B) PC1 vs. PC2 with outliers removed for T3 and T9. Samples cluster within time. (C) PC1 vs. PC4 (T3 and T9 outliers) removed shows clear separation between treatment groups (control and treated). Note: Gene expression was background corrected using the normexp method and then normalized using quantile normalization.

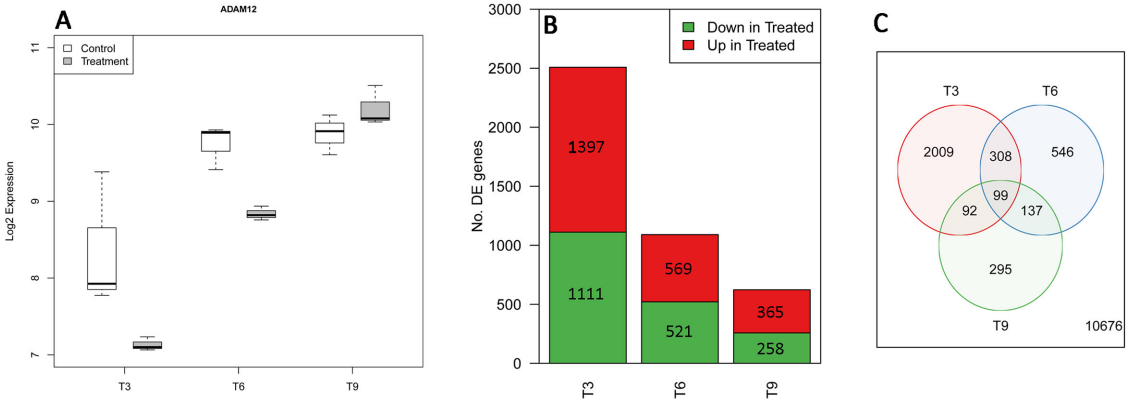

FIGURE 5: Summary of differentially expressed genes in ADAM12 RNAi–treated adipocytes. ADAM12 gene knockdown in ADAM12 RNAi cells compared with control for each time point (T3: day 3 posttransfection; T6: day 6 posttransfection; T9: day 9 posttransfection). (A) Gene knockdown of ADAM12 diminishes with time. (B) Summary of differentially expressed genes up- and down-regulated in ADAM12 RNAi vs. control cells over time (T3, T6, and T9). The biggest impact of ADAM12 gene knockdown on the number of differentially expressed genes was at T3, followed by T6 and T9, respectively. (C) Venn diagram detailing the number of genes differentially expressed in ADAM12 RNAi–treated 3T3-L1 cells vs. control cells, for genes changing at T3, T6, and T9. Values in overlap represent the number of genes found to be different in more than one comparison. T3 and T6 showed the greatest number of genes showing overlap of differentially expressed genes in ADAM12 RNAi cells. $n = 3$ for control and ADAM12 RNAi at each time point.

top-ranked pathway at T9, suggesting the effects of ADAM12 gene knockdown were maintained even though there was little difference in the gene expression of ADAM12 at T9. Gene expression of Igfbp3 (T3, 0.98-fold; ALL, 0.53-fold) and Igfbp5 (T6, 0.36-fold; ALL, 0.53-fold) was increased in ADAM12 RNAi cells. Validation by qRT-PCR confirmed the gene expression of Igfbp3 (see Figure 10A later in the paper) to be up-regulated at T3 and T6 and Igfbp5 (see Figure 10B later in the paper) up-regulated at T6 ($p < 0.05$).

The metabolic pathways found to be differentially regulated that may contribute to altered G3PDH and FAS activity were PPAR signaling, mitochondrial fatty-acid beta oxidation, glucose metabolism, and fatty-acid metabolism. These pathways were all

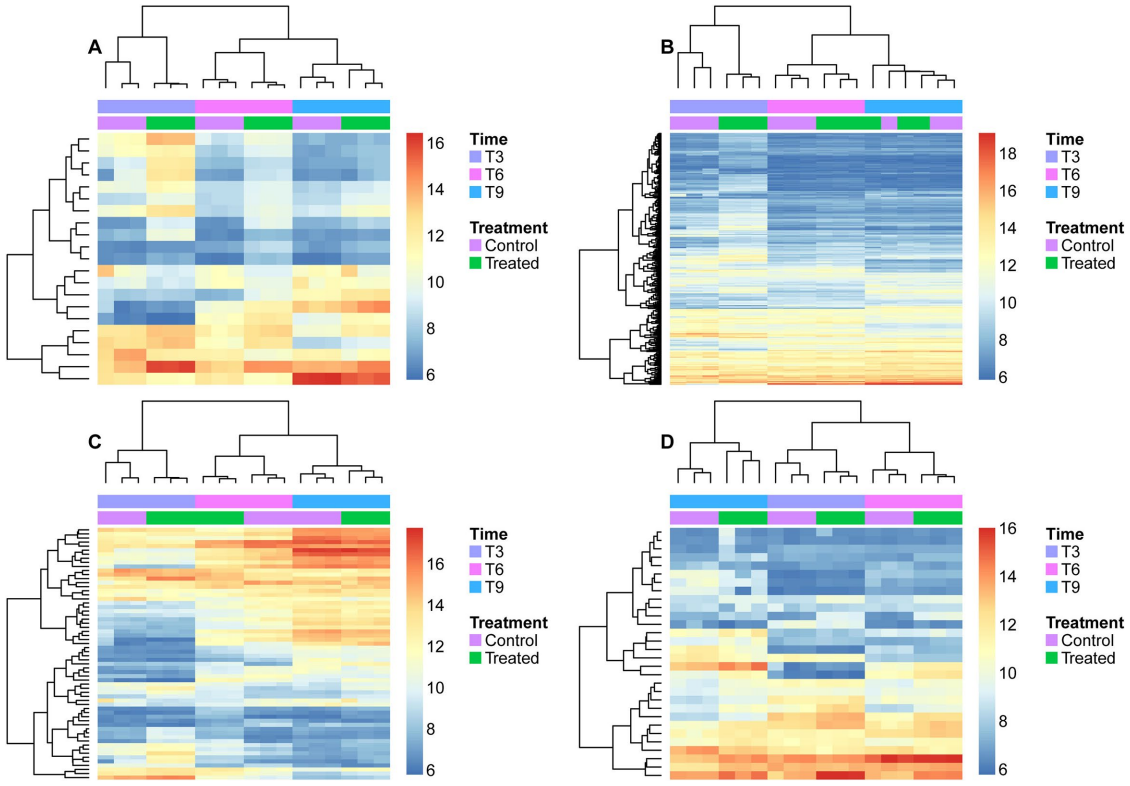

FIGURE 6: Hierarchical clustering of the top differentially regulated genes for each comparison FDR <0.05 and fold change > 2. Genes consistently changing at all time points (A) ALL (T3, T6, and T9), (B) T3, (C) T6, and (D) T9 (T3: day 3 posttransfection; T6: day 6 posttransfection; T9: day 9 posttransfection). $n = 3$ for control and ADAM12 RNAi at each time point.

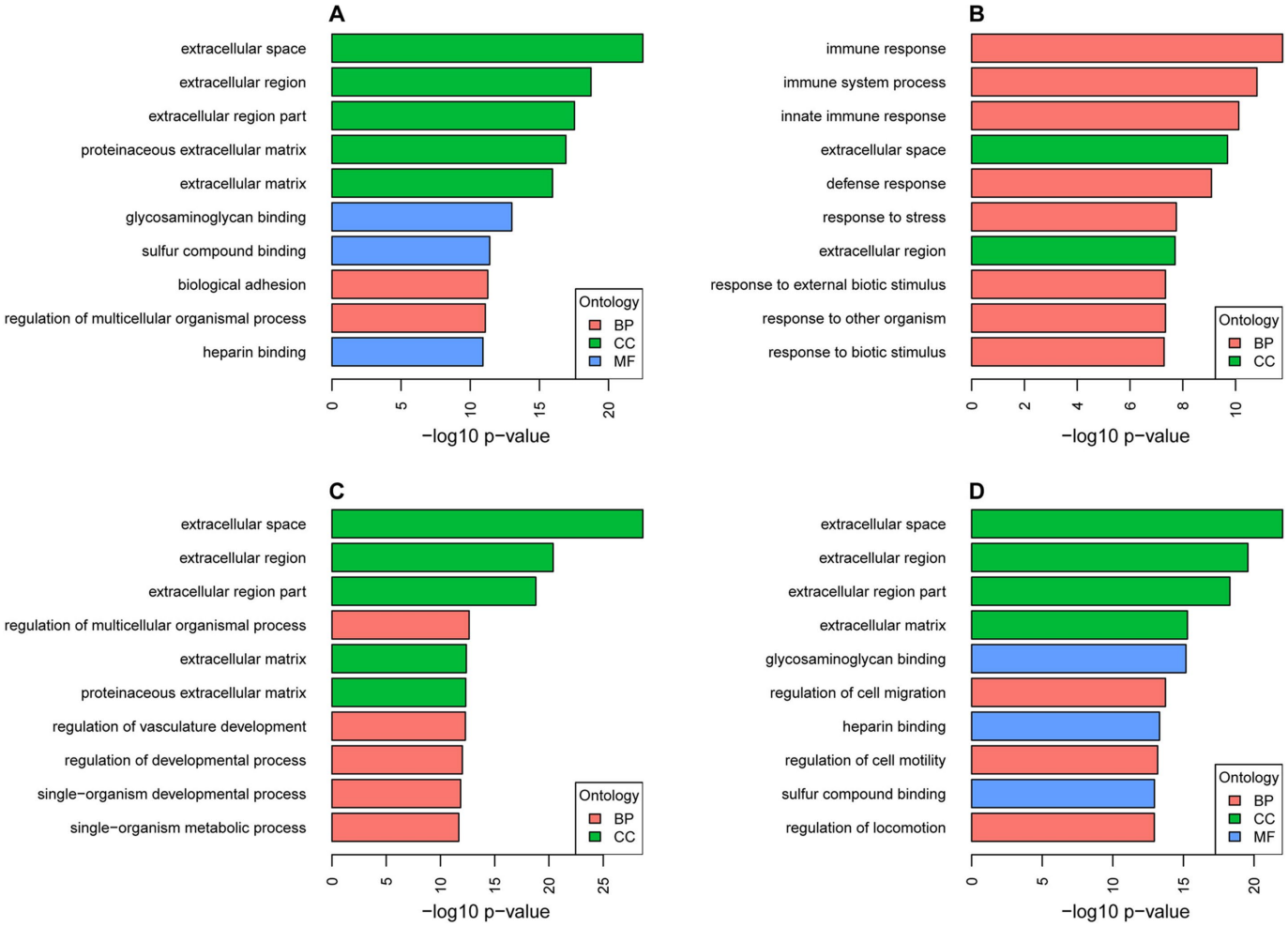

FIGURE 7: Results of gene ontology (GO) analysis of differentially regulated genes in ADAM12 RNAi cells for (A) ALL (across all three time points T3, T6, and T9), (B) T3 (day 3 in culture posttransfection), (C) T6 (day 6 in culture posttransfection), and (D) T9 (day 9 in culture posttransfection). ADAM12 was found to primarily impact the extracellular space/matrix, with the top five GO terms for ALL, T6, and T9 related to this ontology. For T3 the top five GO terms were related to the immune system/response. MF: molecular function; CC: cellular compartment; BP: biological process. $n = 3$ for control and ADAM12 RNAi at each time point.

down-regulated in ADAM12 RNAi cells suggesting that ADAM12 may have a role to play in these processes. Several pathways related to the ECM were up-regulated in ADAM12 RNAi cells at multiple time points: degradation of the extracellular matrix; keratan sulfate degradation for the ALL comparison; and keratan sulfate degradation, keratan sulfate keratin metabolism, and extracellular matrix organization at T9.

The GO analysis at T3 highlighted GO terms for "immune response." Three of the top six pathways at T3 were related to an immune response: interferon alpha beta signaling, interferon gamma signaling, and interferon signaling. Other immune-related pathways were chemokine receptors bind chemokines (ALL, T9), graft versus host disease (T6), and allograft rejection (T6).

Based on the results of our analysis, it appears that ADAM12 is either directly or indirectly influencing numerous pathways during adipogenesis. The main pathway impacted by ADAM12 RNAi in adipocytes was regulation of IGF activity by IGFBPs (Figure 9A). This pathway was found to be up-regulated, and qRT-PCR confirmed gene expression of *Igfbp3* (T3, T6) and *Igfbp5* (T6) were elevated in ADAM12RNAi cells. The mechanism behind this is not apparent from this study, but the absence of cleavage of IGFBP3 and IGFBP5 by ADAM12 knockdown could be driving a positive feedback loop to increase the molecules responsible for activating the regulation of IGFBPs (to release IGF if it is still being bound). This is supported by down-regulation of the IGF/mTOR pathway ($p < 0.05$; Figure 9F) and the mTOR pathway ($p = 0.06$; Figure 9I) as IGF/mTOR signaling is a major growth pathway, which could explain the reduced cell numbers found in ADAM12 RNAi cells. Up-regulation of IGF/mTOR has previously been implicated in positive regulation of PPAR. The PPAR signaling pathway ($p < 0.001$; Figure 9B), *Pparg* (Figure 10E; REML treatment effect, $p < 0.05$), and *Cebpb* (Figure 10F; T3, $p < 0.05$) were also found to be down-regulated. In addition, IGFBP3 can regulate the transcription of adiponectin, an adipocytokine important for fatty-acid oxidation through activation of AMPK (adenosine monophosphate-activated protein kinase). The adipocytokine signaling pathway ($p < 0.05$; Figure 9G), mitochondrial fatty-acid oxidation ($p < 0.001$; Figure 9D), and AMPK-stimulated fatty-acid oxidation pathways ($p = 0.051$; Figure 9H) were down-regulated suggesting a role for ADAM12 in their regulation. The mean normalized gene expression of two adipocytokines *Adipoq* (Figure 10G) and *Cdf* (Figure 10H) showed these genes were down-regulated at T6 and T3 and T6 and T9, respectively ($p < 0.05$). We propose that

Gene description	GenBank accession number	Log fold change
ALL		
Connective tissue growth factor (Ctgf)	NM_010217	1.08
Microfibrillar-associated protein 5 (Mfap5)	NM_015776	1.03
Fibrillin 1 (Fbn1)	NM_007993	0.94
Decorin (Dcn)	NM_007833	0.87
Fibulin 7 (Fbln7)	NM_024237	0.84
Collagen, type V, α3 (Col5a3)	NM_016919	–0.60
Laminin, α5 (Lama5)	NM_001081171	–0.50
SPARC-like 1 (Sparcl1)	NM_010097	–0.50
Nephrocan (Nepn)	NM_025684	–0.43
Cysteine-rich with EGF-like domains 1 (Creld1)	NM_133930	–0.40
T3		
Connective tissue growth factor (Ctgf)	NM_010217	2.37
Von Willebrand factor homologue (Vwf)	NM_011708	1.80
Bone γ-carboxyglutamate protein 2 (Bglap2)	NM_001032298	1.44
Microfibrillar-associated protein 5 (Mfap5)	NM_015776	1.23
Dermatopontin (Dpt)	NM_019759	1.20
Collagen, type V, α2 (Col5a2)	NM_007737	–1.28
Transforming growth factor, β induced (Tgfbi)	NM_009369	–1.24
SPARC-like 1 (Sparcl1)	NM_010097	–0.95
Collagen, type IV, α5 (Col4a5)	NM_001163155	–0.91
Collagen, type XI, α1 (Col11a1)	NM_007729	–0.90
T6		
Connective tissue growth factor (Ctgf)	NM_010217	1.20
Osteoglycin (Ogn)	NM_008760	1.03
Microfibrillar-associated protein 5 (Mfap5)	NM_015776	1.02
Keratocan (Kera)	NM_008438	0.94
Lumican (Lum)	NM_008524	0.93
Collagen, type V, α3 (Col5a3)	NM_016919	–0.89
Laminin, α5 (Lama5)	NM_001081171	–0.75
Nephrocan (Nepn)	NM_025684	–0.69
Collagen, type IV, α2 (Col4a2)	NM_009932	–0.60
Collagen, type VI, α3 (Col6a3)	NM_133930	–0.52
T9		
Fibulin 7 (Fbln7)	NM_024237	1.39
Matrix Gla protein (Mgp)	NM_008597	1.00
Keratocan (Kera)	NM_008438	0.98
Osteoglycin (Ogn)	NM_008760	0.96
AE binding protein 1 (Aebp1)	NM_001291857	0.94
Laminin, β3 (Lamb3)	NM_008484	–0.77
Nephrocan (Nepn)	NM_025684	–0.43

T3: day 3 in culture posttransfection; T6: day 6 in culture posttransfection; T9: day 9 in culture posttransfection; ALL: across all three time points T3, T6, and T9. n = 3 for control and ADAM12 RNAi at each time point. The top five up-regulated and down-regulated genes are presented (FDR < 0.05 and |FC| > 2). Magnitude of regulation is based on fold change.

TABLE 1: Core-matrisome genes (Naba *et al.*, 2012) differentially expressed in ADAM12 RNAi cells across all time points (ALL), T3, T6, and T9.

Signaling pathways	No. of genes	Direction	*p* value
ALL			
Regulation of insulin-like growth factor (IGF) activity by insulin-like growth factor binding proteins (IGFBPs)	26	UP	2.90E-07
PPAR signaling	51	DOWN	1.24E-06
Branched chain amino acid catabolism	17	DOWN	1.26E-06
Valine leucine and isoleucine degradation	45	DOWN	1.32E-06
Chemokine receptors bind chemokines	23	UP	1.94E-06
Degradation of the extracellular matrix	34	UP	3.17E-06
Keratan sulfate degradation	12	UP	8.90E-06
Mitochondrial fatty-acid beta oxidation	15	DOWN	9.07E-06
Glucose metabolism	54	DOWN	6.05E-05
Fatty-acid metabolism	37	DOWN	6.54E-05
T3			
Interferon alpha beta signaling	82	DOWN	2.53E-11
Interferon gamma signaling	70	DOWN	4.57E-10
Cholesterol biosynthesis	16	UP	5.87E-08
Endosomal vacuolar pathway	20	DOWN	1.32E-06
Interferon signaling	168	DOWN	6.75E-06
VITCB pathway	18	DOWN	1.44E-05
T6			
PPAR signaling pathway	51	DOWN	3.17E-08
Valine leucine and isoleucine degradation	45	DOWN	1.13E-06
Graft vs. host disease	28	UP	1.18E-06
Allograft rejection	29	UP	1.59E-06
Branched chain amino acid catabolism	17	DOWN	3.13E-06
CTL pathway	27	UP	4.36E-06
T9			
Regulation of insulin-like growth factor (IGF) activity by insulin-like growth factor binding proteins (IGFBPs)	26	UP	6.76E-08
Keratan sulfate degradation	12	UP	4.65E-07
Glycosaminoglycan metabolism	82	UP	3.66E-06
Keratan sulfate keratin metabolism	24	UP	4.22E-06
Extracellular matrix organization	74	UP	5.16E-06
Chemokine receptors and chemokines	23	UP	6.09E-06

T3: day 3 in culture posttransfection; T6: day 6 in culture posttransfection; T9: day 9 in culture posttransfection; ALL: across all three time points T3, T6, and T9. $n = 3$ for control and ADAM12 RNAi at each time point.

TABLE 2: Top signaling pathways differentially regulated in ADAM12 RNAi cells across all comparisons (ALL), T3, T6, and T9.

these pathways interact during adipogenesis as a direct result of the absence/reduction of cleavage of IGFBP3 and IGFBP5 by ADAM12.

DISCUSSION

Previous studies on ADAM12 have shown it is involved in adipogenesis (Kawaguchi *et al.*, 2002, 2003; Kurisaki *et al.*, 2003; Masaki *et al.*, 2005). We wanted to use an established model of adiponenesis in vitro to investigate this further. Using metabolic markers of adipocyte differentiation and gene profiling we were able to more clearly define pathways involved in regulation of adipogenesis and identify novel pathways for ADAM12 during adipogenesis. 3T3-L1 cells proliferate as a flat-fibroblastic–appearing preadipocyte. Following clonal expansion, the cells arrest and differentiate into a round adipocyte. Following the early stage of differentiation, cells begin lipid-filling to become mature adipocytes. The primary role of this mature adipocyte is to store energy and break down fatty acids to provide ATP when available systemic sources become low. During the course of development the ECM serves as a structure to support the large changes in cell morphology and to harvest and sequester ligands important for signaling proliferation and differentiation.

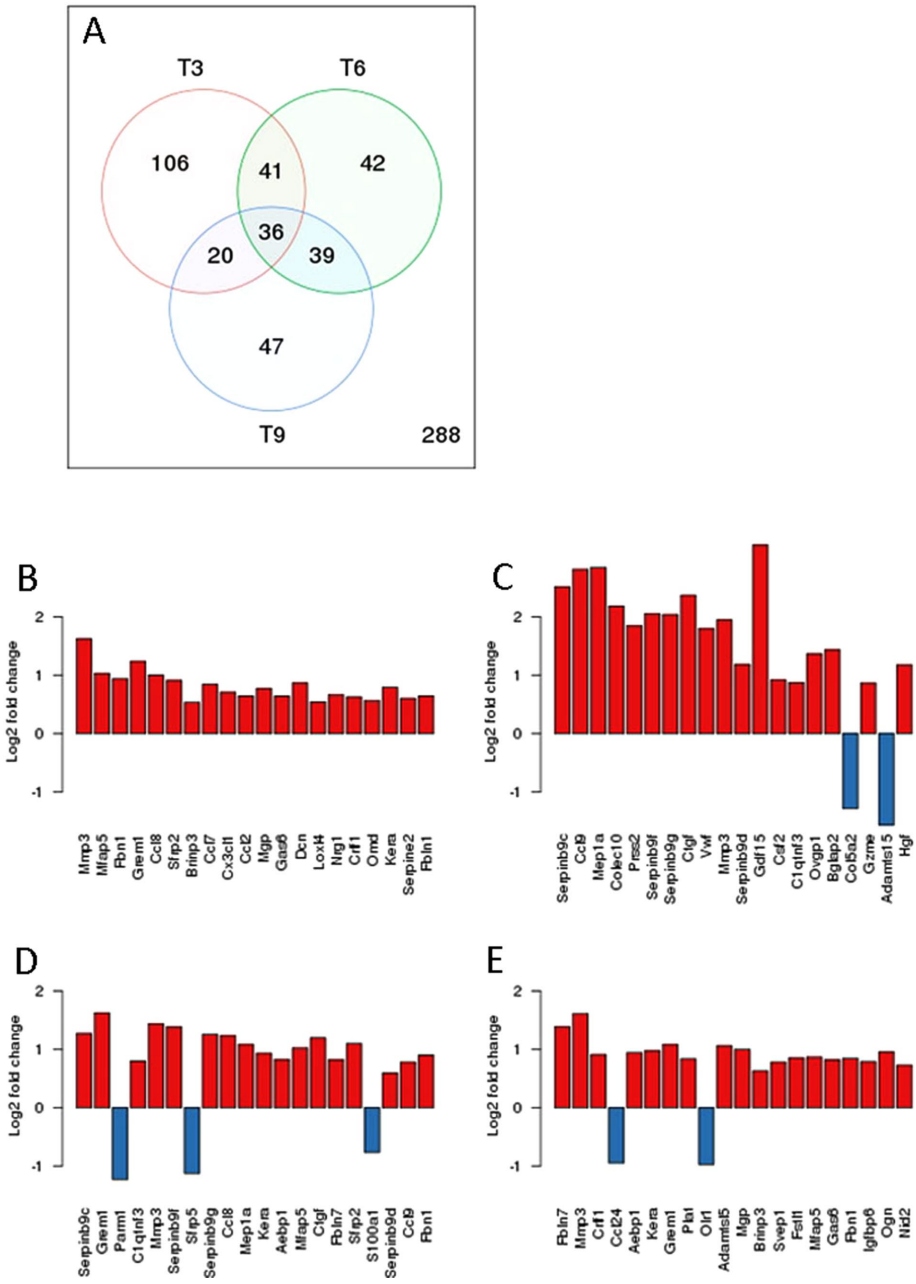

FIGURE 8: The effect of ADAM12 gene knockdown on gene expression of matrisome genes. (A) Venn diagram detailing the number of matrisome genes (including 177 core-matrisome and 444 matrisome-associated genes) differentially expressed in ADAM12 RNAi–treated 3T3-L1 cells vs. control cells, for genes changing at T3, T6, and T9. Values in the overlap represent the number of genes found to be different in more than one comparison. T3 and T6 showed the greatest number of overlapping differentially expressed genes in ADAM12 RNAi cells. (B–E) Top-ranked matrisome genes (FDR <0.05) for ALL, T3, T6, and T9; bar plots reflect the magnitude of change expression between treated and control cells (log_2-fold change). *Mmp3* is top ranked for all comparisons. Core-matrisome genes *Mfap5*,*Fbn1*, and *Ctgf* remain as top ranked for ALL, T6, and T9 (*Mfap5*,*Fbn1*) and T3 and T6 (*Ctgf*). *Mmp3*: matrix metalloprotease 3; *Mfab5*: microfibrillar-associated protein 5; *Fbn1*: fibrillin 1; *Ctgf*: connective tissue growth factor. $n = 3$ for control and ADAM12 RNAi at each time point.

ADAM12 is an active protease in the ECM; we have identified pathways ADAM12 influences in the ECM to cause changes in proliferation and differentiation during the course of adipocyte maturation. GO analysis revealed the ECM as being a major compartment of the cell where ADAM12 was impacting. Using genes consistently changing across all time points (ALL gene list), we found the pathway most significantly affected by ADAM12 gene knockdown was regulation of IGF activity by IGFBPs. In vitro studies have shown ADAM12-S binds and cleaves IGFBP3 and IGFBP5 (Loechel *et al.*, 2000; Shi *et al.*, 2000). The main function of IGFBPs is to bind IGF-1 and IGF-2, transport them extracellularly, and protect them from degradation (increasing their half-life; Ruan and Lai, 2010). Once the IGFs are released from IGFBP, they can bind to their IGF receptors (IGFr) and induce IGF-IGFr mediated signaling within the cell, such as induction of cell proliferation (Rajkumar *et al.*, 1999; Firth and Baxter, 2002). Although IGFs are bound to IGFBPs, they can inhibit cell growth by reducing the bioavailability of IGFs to their receptors to regulate cellular activity. Activation of this pathway is consistent with reduced cell numbers in ADAM12 RNAi cells on days 3, 6, and 9. It is plausible knockdown of ADAM12 reduced cleavage of IGFBP3 and IGFBP5 to inhibit release and bioavailability of IGF in the ECM, impeding proliferation to result in reduced cell numbers. In turn, this potentially initiates a feedback loop to increase expression of IGFBPs and other molecules in the pathway responsible for cleavage of IGFBPs to cause it to be up-regulated. In addition, we found downstream signaling pathways of IGF to be affected; these included down-regulation of the IGF/mTOR signaling pathway. IGF/IGFR induces growth through the PI(3)K/Akt/mTOR signaling axis (Bodine *et al.*, 2001; Rommel *et al.*, 2001; Floyd *et al.*, 2007; Laplante and Sabatini, 2012). Suppression of the mTOR signaling pathway suggests that IGF ligand binding to IGFR was affected. This data is in support of previous findings where adipocytes isolated from inguinal white adipose tissue (WAT; a fat depot of high proliferative capacity) of ADAM12–/– mice fed a high-fat diet had reduced cell numbers compared with wild-type mice (Masaki *et al.*, 2005). Collectively these data suggest a role for ADAM12 in proliferation during adipogenesis. Based on these results, a working model of how ADAM12 stimulates proliferation through the IGF/mTOR signaling pathway is provided (Figure 11). In the absence of ADAM12, cleavage of IGFBPs is hindered, in particular its substrates IGFBP3 and IGFBP5, inhibiting release of IGF and reducing its bioavailability to IGFR. This impacts downstream signaling of the mTOR signaling pathway impeding proliferation of preadipocytes.

Three of the top five signaling pathways differentially regulated when preadipocytes were proliferating and knockdown of ADAM12 gene expression was the greatest (day 3) were related to IFN (interferon) signaling, interferon alpha beta signaling, interferon

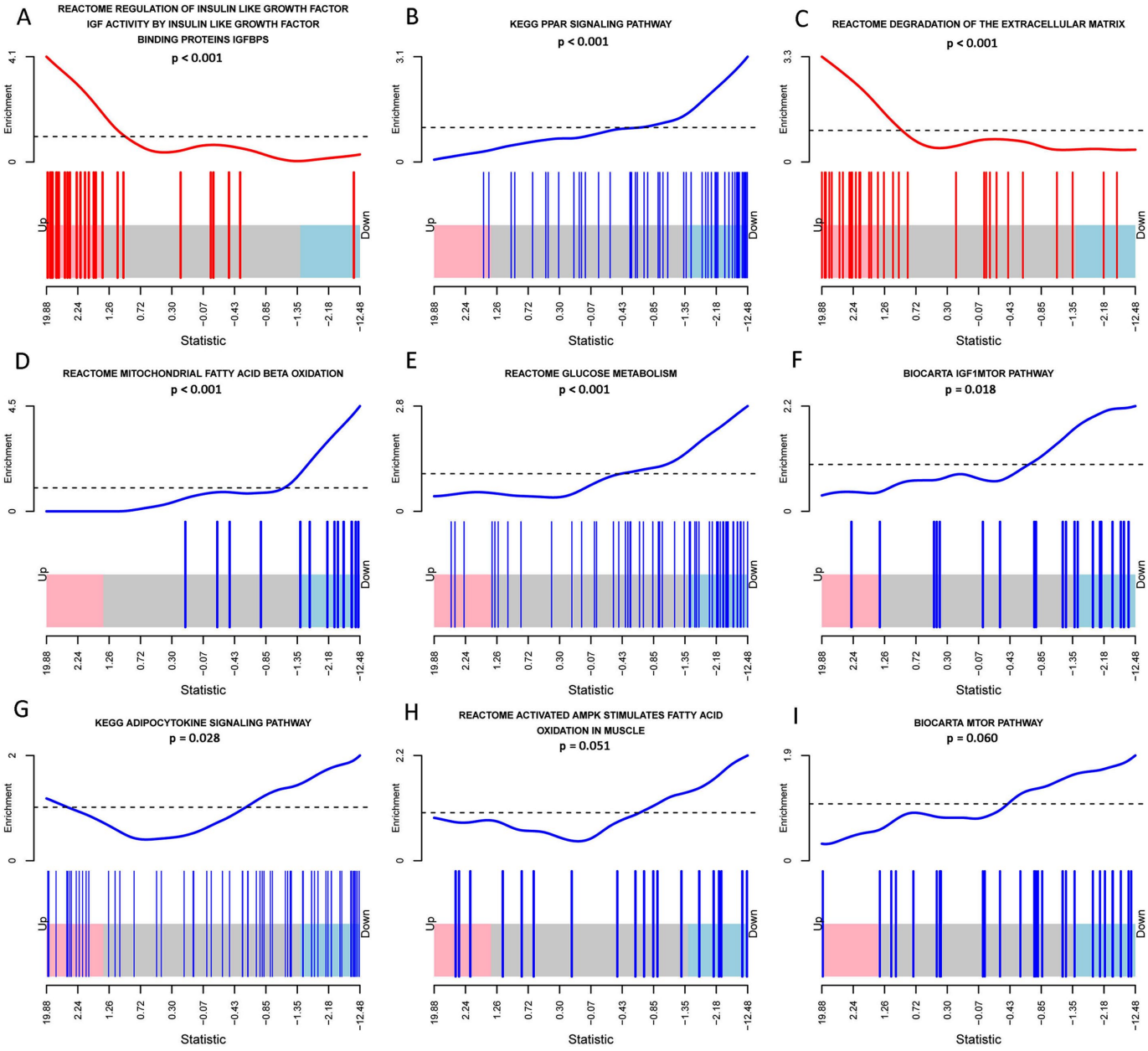

FIGURE 9: Barcode plots for a selection of growth signaling pathways differentially regulated in ADAM12 RNAi cells (ALL comparison across all time points T3, T6, and T9). (A) Regulation of insulin-like growth factor (IGF) activity by insulin-like growth binding proteins IGFBPs and (C) degradation of the extracellular matrix were up-regulated with ADAM12 gene knockdown. Pathways down-regulated which are potentially acting antagonistically or down-regulated in response to up-regulation of A were (B) PPAR signaling pathway, (D) mitochondrial fatty-acid beta oxidation, (E) glucose metabolism, (F) IGF/mTOR pathway, (G) adipocytokine signaling pathway, (H) activated AMPK (adenosine monophosphate-activated protein kinase) stimulated fatty-acid oxidation, and (I) mTOR pathway. *n* = 3 for control and ADAM12 RNAi at each time point.

gamma signaling, and interferon signaling. IFNs can act as negative regulators of proliferation by blocking the transition from G_0/G_1 into the S phase of the cell cycle (Clemens and McNurlan, 1985; Hertzog *et al.*, 1994). IFNα (alpha), IFNβ (beta), and IFNγ (gamma) have been found to be potent inhibitors of cell proliferation (Clemens and McNurlan, 1985; Hertzog *et al.*, 1994). All three IFN pathways were down-regulated in proliferating ADAM12 RNAi preadipocytes. It is not clear from this study whether suppression of IFN signaling is in response to impeded cell growth as a mechanism to maintain proliferation or if ADAM12 directly impacts IFN signaling by remodeling of the ECM or via direct interaction. This is of further interest as both ADAM12 and IFNs are modulated in tumor growth (Clemens and McNurlan, 1985; Hertzog *et al.*, 1994; Kveiborg *et al.*, 2008).

Following proliferation and growth arrest of preadipocytes, we investigated the effect of ADAM12 knockdown on enzymatic markers of differentiation. The activity of G3PDH was increased from day 6 to day 15 and FAS was elevated at day 9 in ADAM12 RNAi cells. We also measured when preadipocytes differentiated to round adipocytes, the size of mature lipid-filled adipocytes, and the size of large lipid droplets in mature adipocytes. We found on day 9 that the

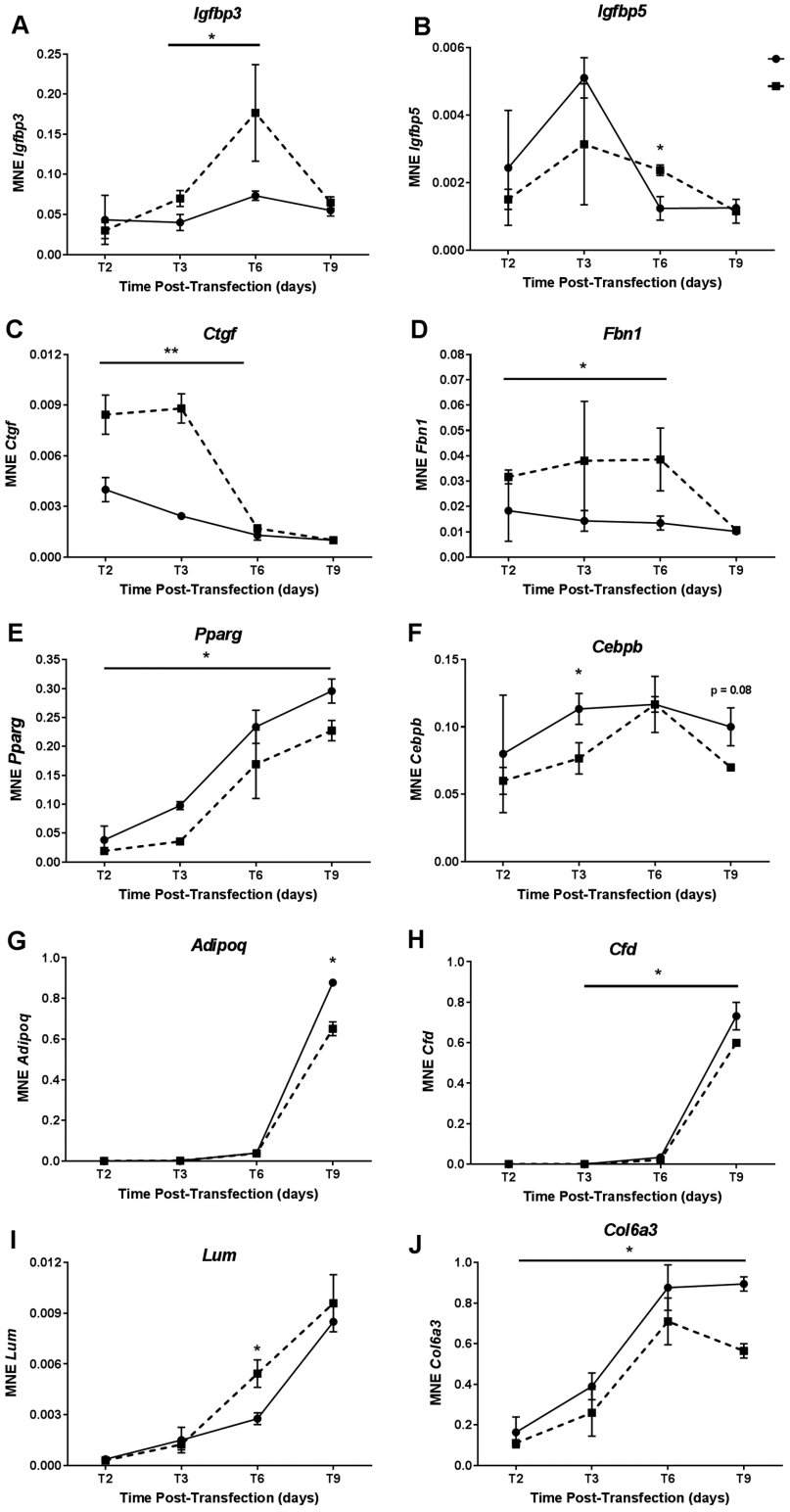

FIGURE 10: Validation of microarray gene expression by quantitative real-time PCR (qRT-PCR). Mean normalized gene expression (MNE) of (A) *Igfbp3*, (B) *Igfbp5*, (C) *Ctgf*, (D) *Fbn1*, (E) *Pparg*, (F) *Cebpb*, (G) *Adipoq*, (H) *Cdf*, (I) *Lum*, and (J) *Col6a3* using *Ppia* as the housekeeping gene. *Igfbp3*: insulin-like growth factor binding protein 3; *Igfbp5*: insulin-like growth factor binding protein 5; *Ctgf*: connective tissue growth factor; *Fbn1*: fibrillin 1; *Pparg*: peroxisome proliferator–activated receptor gamma; *Cebpb*: CCAAT/enhancer binding protein beta; *Adipoq*: adiponectin; *Cfd*: complement factor D (adipsin); *Lum*: lumican; *Col6a3*: collagen type VI alpha 3 chain; *Ppia;* peptidylprolyl isomerase A (cyclophilin A). Note: These data are from a trial independent to the microarray. *, $p < 0.05$; **, $p < 0.01$ ($n = 3$ for control and ADAM12 RNAi at each time point).

number of preadipocytes was greater in ADAM12 RNAi cells and there were less adipocytes, suggesting differentiation was delayed. Also on day 9 the mean diameter of control adipocytes was close to being greater than ADAM12 RNAi cells ($p = 0.057$) and cells with two lipid droplets were smaller in ADAM12 gene knockdown cells. On day 13, the size of adipocytes was not different in ADAM12 RNAi cells but the size of lipids in cells with one, two, and three lipid droplets was found to be greater. These results suggest differentiation is delayed and either lipogenesis is enhanced or fatty-acid oxidation is impeded in ADAM12 RNAi cells to cause elevated activity of G3PDH/FAS and increased accumulation of lipids in mature adipocytes. Other authors have implicated a role for ADAM12 during differentiation (Kawaguchi *et al.*, 2003; Masaki *et al.*, 2005). Kawaguchi *et al.* (2003) found ADAM12 induced actin cytoskeleton reorganization and caused 3T3-L1 cells to become less adhesive to the ECM via regulation of β1 integrin and reorganization of the dense fibronectin-rich matrix during differentiation of flat preadipocytes to rounded adipocytes. Mouse embryonic fibroblasts from ADAM12–/– mice also showed impaired differentiation (and proliferation) after hormonal treatment to induce differentiation (Masaki *et al.*, 2005). Reorganization of the fibronectin-rich matrix during preadipocytes differentiation is one explanation for ADAM12 involvement in this as it has been shown to cleave fibronectin (Roy *et al.*, 2004). In addition, the matrisome gene *Fbn1* (fibrillin-1) was up-regulated during proliferation and differentiation of ADAM12 RNAi adipocytes. Up-regulation of *Fbn1* was found in the adipose tissue of obese women and associated with increased adipocyte size (Davis *et al.*, 2016); it may have influenced increased lipogenesis in ADAM12 RNAi cells. A role for IGFBP3 is also possible as it has been implicated in inhibition of preadipocyte differentiation and further development of adipocyte differentiation (Baxter and Twigg, 2009). PPARγ is known as the master regulator of adipogenesis, responsible for inducing expression of adipogenic genes involved in adipose cell differentiation (Brun *et al.*, 1996). Recombinant human IGFBP3 interacts with PPARγ; this interaction was found to inhibit RXRα-PPARγ transcriptional activity, affecting a large number of PPARγ-regulated genes (Chan *et al.*, 2009; Lefterova and Lazar, 2009). The second top pathway in the ALL gene list to be affected by ADAM12 knockdown was PPARγ signaling. qRT-PCR found *Pparg* was down-regulated through the course of proliferation and differentiation. With the potential of reduced

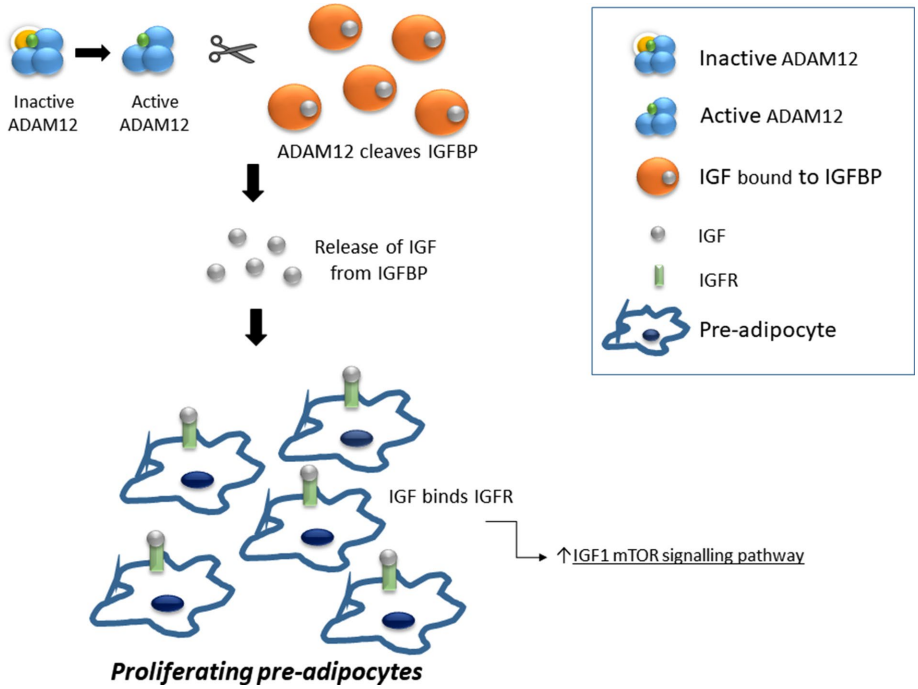

FIGURE 11: Working model for ADAM12 during proliferation in preadipocytes. Active ADAM12 cleaves IGFBP3 and IGFBP5 to release the potent regulator of growth IGF into the extracellular matrix (Loechel *et al.*, 2000). IGF is free to bind to IGFR on the cell surface stimulating proliferation of preadipocytes through the mTOR signaling pathway. Knockdown of ADAM12 results in reduced proliferation and regulation of the IGF1 mTOR signaling pathway. We propose knockdown of ADAM12 results in reduced cleavage of IGFBP, particularly IGFBP3 and IGFBP5, to make IGF1 available to IGFR on the cell surface reducing mTOR signaling and proliferation of preadipocytes. (ADAM12: a disintegrin and metalloprotease 12; IGFBP3: insulin-like growth factor binding protein 3; IGFBP5: insulin-like growth factor binding protein 5; IGF: insulin growth factor; IGFR: insulin growth factor receptor; mTOR: mechanistic target of rapamycin).

IGFBP3 cleavage in ADAM12 RNAi cells and increased expression, we observe from day 3 to day 9 during the fundamental stages of differentiation that it is possible IGFBP3 could be impairing differentiation by hampering the RXRα/PPARγ interaction to reduce induction of PPARγ-regulated genes and therefore the PPARγ signaling pathway. Mice overexpressing ADAM12 found PPARγ was up-regulated in developing adipocytes found within connective tissue of skeletal muscle further supporting a role for ADAM12 in PPARγ signaling (Kawaguchi *et al.*, 2003).

Similarly, connective tissue growth factor (CTGF) shows many parallels with IGFBP3, also reported to inhibit differentiation in 3T3-L1 cells (Tan *et al.*, 2008). *Ctgf* was up-regulated in ADAM12 RNAi cells (ALL, T3, and T6); validation by qRT-PCR confirmed this at T2 and T3. CTGF inhibits adipocyte differentiation by targeting CCAAT/enhancer binding protein-β (C/EBPβ) to block PPARγ. Gene expression of *Cebpb and Pparg* were down-regulated in ADAM12 RNAi cells suggesting PPARγ signaling was impacted. CTGF up-regulates tissue inhibitor of matrix metalloproteases 1 (TIMP-1; McLennan *et al.*, 2004); TIMP-1 blocks cleavage of IGFBP3 by matrix metalloproteases (MMP1, MMP2, and MMP3; Fowlkes *et al.*, 1994) inhibiting proteolysis of IGFBP3 by other MMPs. *Mmp3* was up-regulated (ALL, T3, T6, and T9); however, *Timp1* (ALL, T6, and T9), *Timp2* (ALL, T6, and T9), and *Timp3* (T6) also had increased gene expression, potentially induced by increased *Ctgf* which could hinder any compensatory cleavage of IGFBP3. The inverse relationship that *Igfbp3* and *Ctgf* have with ADAM12 gene expression and their potential impact on PPARγ signaling is unknown but is of further interest.

Increased lipogenesis found in ADAM12 RNAi cells as observed by elevated G3PDH, FAS, and larger lipids in mature adipocytes suggests that lipogenesis is dominating over fatty-acid oxidation. We found the mitochondrial fatty-acid beta oxidation pathway (ALL gene list) to be down-regulated. Linked to this, adipocytokine signaling pathway and activated AMPK stimulates fatty-acid oxidation were also down-regulated (ALL gene list). As mentioned above, IGFBP3 can interfere with regulation of PPARγ-regulated genes; the adipocytokine adiponectin (*Adipoq*) is one of them (Zappala and Rechler, 2009). IGFBP3 can inhibit expression of *Adipoq* via interaction with PPARγ (Zappala and Rechler, 2009). Adiponectin is an energy sensing cytokine which stimulates AMPK to increase fatty-acid oxidation, reducing the triglyceride content of adipocytes in adipose tissue and skeletal muscle when energy is low. Reduced expression of adiponectin and another adipocytokine, *Cfd* (adipsin), is associated with hypertrophy of adipocytes in obesity and insulin resistance in obesity and type II diabetes (Rosen *et al.*, 1989; Kadowaki and Yamauchi, 2005; Zappala and Rechler, 2009). The gene expression of *Adipoq* and *Cfd* was decreased in ADAM12 RNAi adipocytes (qRT-PCR). Other adipocytokines that regulate AMPK-stimulated fatty-acid oxidation that may have caused these pathways to be down-regulated are leptin and IL-6; however, these were not differentially regulated in ADAM12 RNAi cells. Further studies are required to determine what is driving increased lipogenesis and reduced signaling of fatty-acid oxidation pathways as a result of ADAM12 gene knockdown. We believe reduced PPARγ signaling due to increased expression of *Igfbp3* and *Ctgf* and potentially reduced cleavage of IGFBP3 may be altering adipocytokine and downstream fatty-acid oxidation pathways. As a result, lipids accumulate in ADAM12 RNAi cells; a working model is provided in Figure 12.

Previous findings in ADAM12 knockout mice and mice overexpressing ADAM12 suggest ADAM12 promotes adipogenesis in vivo. However, in our study, we show that ADAM12 knockdown in vitro increases lipid accumulation. This result may not be representative in vivo due to other tissues able to secrete molecules such as adipocytokines which can then be made available to adipocytes. For example, adiponectin is also expressed by muscle (Krause *et al.*, 2008), potentially making it available to bind to adiponectin receptors on adipocytes. This could counteract the impaired adipocytokine signaling we see in ADAM12 RNAi cells. We also believe that the effects of ADAM12 on adipogenesis in vivo are predominantly driven by the impact on proliferation through IGF/mTOR signaling as this was the top pathway affected in vitro as described above.

Final remarks

Mice overexpressing ADAM12 have increased adipocytes within skeletal muscle (Kawaguchi *et al.*, 2002) and in the absence of ADAM12, mice are resistant to a high-fat diet (Masaki *et al.*, 2005)

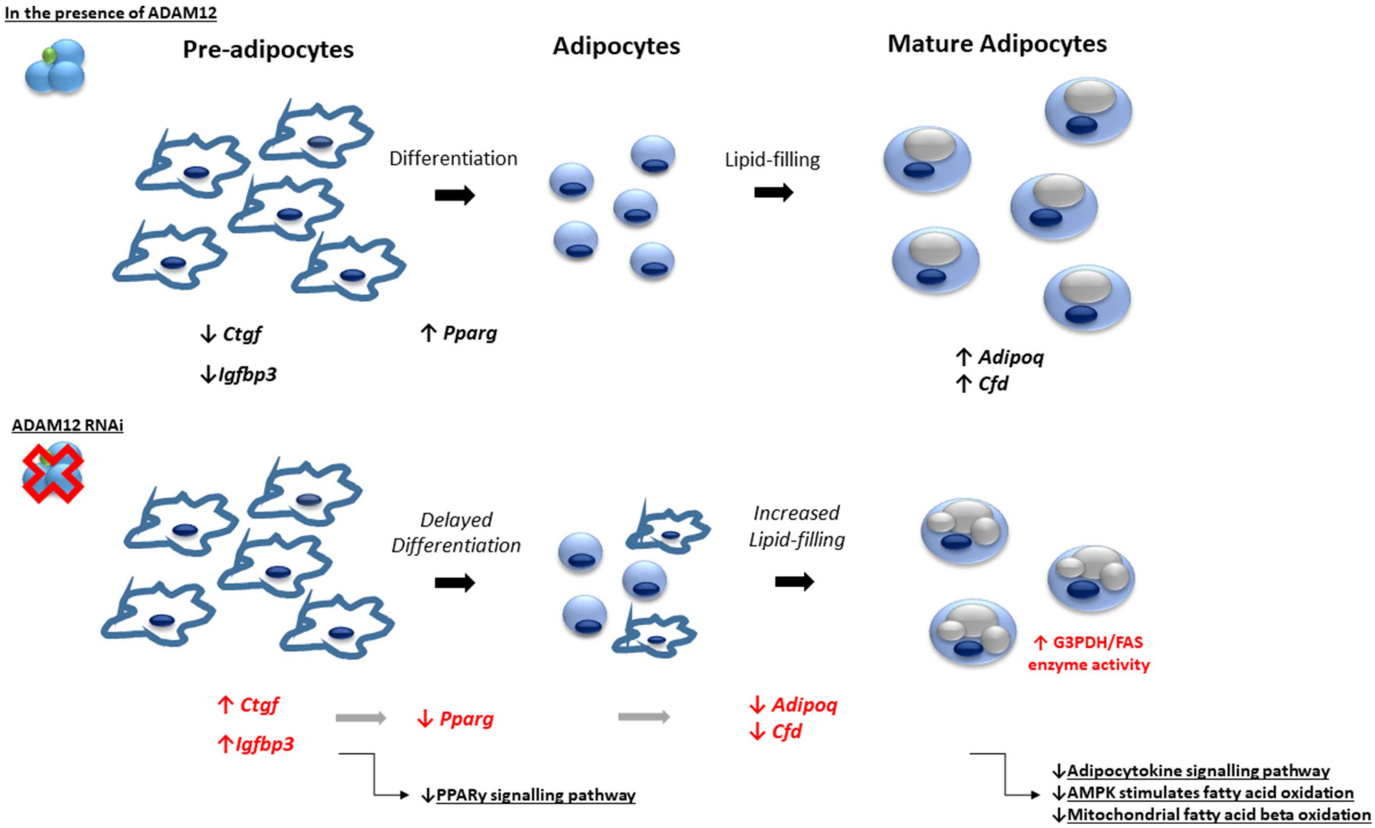

FIGURE 12: Working model for ADAM12 during differentiation of preadipocytes and maturation of adipocytes. In the presence of ADAM12, PPARγ—the master regulator of adipogenesis—stimulates genes for adipocytes to differentiate changing their morphology from a flattened preadipocyte to a round cell. Adipocytes then mature, filling with lipid as a mechanism to store energy. Adipocytokines, such as *Adipoq* and *Cfd,* finely maintain the balance of lipids by sensing when energy is required by other tissues stimulating AMPK fatty-acid oxidation. Knockdown of ADAM12 in vitro causes increased expression of *Igfbp3* and *Ctgf*. Both these molecules are known to inhibit expression of PPARγ, the master regulator of adipogenic differentiation genes. We postulate increased expression of *Igfbp3* and *Ctgf* inhibits expression of PPARγ, reducing its expression to impact negatively on the PPARγ signaling pathway to delay differentiation. Adipocytokines, such as *Adipoq,* control the imbalance of lipids within adipocytes via AMPK-stimulated fatty-acid oxdiation. IGFBP3 can interfere with regulation of *Adipoq* via interaction with PPARγ. Reduced PPARγ may also impede on adipocytokine signaling, down-regulating *Adipoq* expression and consequently AMPK fatty-acid oxidation and mitochondrial fatty-acid beta oxidation signaling pathways. Other adipocytokines, such as *Cfd,* are reduced and may also be affecting the balance of lipids within adipocytes. (ADAM12: a disintegrin and metalloprotease 12; PPARγ: peroxisome proliferator-activated receptor gamma; *Adipoq*: adiponectin; *Cfd*: adipsin; *Igfbp3*: insulin-like growth factor binding protein 3; *Ctgf*: connective tissue growth factor; G3PDH: glycerol-3-phosphate dehydrogenase; FAS: fatty-acid synthase; AMPK: adenosine monophosphate–activated protein kinase).

with reduced interscapular BAT (Kurisaki *et al.*, 2003). We have shown ADAM12 is important for signaling proliferation of preadipocytes, differentiation of flat-fibroblastic preadipocytes into round adipocytes, and for maintaining the balance of lipids within mature adipocytes. This study suggests ADAM12 may control the transcript levels of IGFBP-binding proteins, particularly *Igfbp3* and *Igfbp5*, and other inhibitors of adipocyte differentiation, *Ctgf*, to potentially enable proper gene expression and functioning of PPARγ, the master regulator of adipogenesis. We believe these pathways may be active in vivo to cause increased accumulation of adipocytes within skeletal muscle in transgenic mice overexpressing ADAM12 and resistance to a high-fat diet. Concomitantly, Zhou *et al.* (2013) considered the role of ADAM12 in the cellular reprogramming of embryonic fibroblasts into BAT cells. Induced expression of ADAM12S (and HB-EGF) promoted lipid accumulation and an increase in expression of genes associated with BAT (PRDM16, PGC-1α, UCP-1); the expression of WAT genes was unaltered (PPARγ, C/EBPα, AKT-1) suggesting ADAM12-S influences cellular plasticity of BAT but not WAT cells. The cellular pathways ADAM12S influences to cause reprogramming of embryonic fibroblasts into BAT cells are of interest and may be responsible for reduced interscapular BAT in ADAM12 knockout mice (Zhou *et al.*, 2013).

In addition, ADAM12 is implicated in many cancers, including mammary, bladder, liver, lung, oral, stomach, colon, brain, and bone (Kveiborg *et al.*, 2008). IGFBP/IGF/mTOR signaling by ADAM12 may also be driving tumor growth in these cancers. Pharmalogical inhibitors of ADAM12 may prove beneficial in controlling adipocyte expansion in disorders such as obesity and metabolic disease.

MATERIALS AND METHODS

The cell line used for this study was a well-established murine preadipocyte cell line, 3T3-L1. Each well of a six-well plate was seeded with

1.98×10^4 cells and incubated overnight in DMEM plus 10% fetal bovine serum (FBS) in a humidified CO_2 incubator. Preadipocytes at 80% confluency were transfected using Lipofectamine 2000 (Invitrogen, Australia) with either 20 pmol (in Opti-MEM I Reduced Serum Media without serum or antibiotics) of ADAM12 Stealth RNAi (GCA ACU CCU GUG ACC UCC CAG AAU U) or Stealth RNAi Negative Control Medium GC Duplex #2 (Invitrogen, Australia) as the control as per manufacturers guidelines. Transfection efficiency (>95%) was determined using the BLOCK-iT Flourescent Oligo (Invitrogen, Australia). After 6 h transfection, media was aspirated and replaced with Opti-MEM I Reduced Serum Media plus 10% (vol/vol) FBS. Fresh growth media was added to 3T3-L1 cells every second day. On day 3 cells were placed in differentiation media (DMEM and 10% [vol/vol] FBS, 0.5 mM IBMX, 1 μM dexamethasone, 10 μg/ml insulin, and 10 μg/ml biotin) until cells differentiated. 3T3-L1 adipocytes were then placed in postdifferentiation media on day 9 (DMEM and 10% [vol/vol] FBS plus 10 μg/ml insulin) to accelerate lipid-filling of adipocytes. 3T3-L1 cells were incubated in postdifferentiation media until development of mature adipocytes.

Morphometrics on preadipocytes and adipocytes

Morphometrics were conducted on phase contrast images ($n = 3$ for each treatment/time point) of 3T3-L1 preadipocytes and adipocytes using Leica Microsystems QWin image analysis software (Cambridge, UK), adapted from a previously described method (McDonough *et al.*, 2009). Differentiation was measured by counting the number of preadipocytes (flattened fibroblastic-appearing cell) and adipocytes (rounded cell) in independent images. The proportion of preadipocytes to adipocytes was then calculated (pre-dipocytes/adipocytes). Mature adipocyte development (lipid filling) was determined by first measuring the diameter of adipocytes for each cell present in an independent image ($n = 2$ images). The diameter of lipid droplets contained within adipocytes was also measured for cells containing one, two, and three lipid droplets present in the image. Only adipocytes containing one, two, or three lipid droplets were measured due to the complexity of counting adipocytes containing more than three lipid droplets. Measurements were grouped according to the number of lipid droplets contained within the cell (one, two, and three lipid droplets).

DNA quantitation to assay cell numbers

Cell numbers were measured by the amount of DNA (μg/ml). Cells were lysed with 0.1 M PBS, 50 mM MES, 50 mM trizma base, 1× Triton X-100, and 1 Roche cocktail protease inhibitor tablet and labeled with Sybr Safe (Invitrogen, Australia). The fluorescence in each well was measured using Stratagene Mx3000P (Agilent, Santa Clara, CA) and mean fluorescence for each sample was calculated from DNA standards.

G3PDH and FAS enzyme activity

Two enzyme markers were measured to assess the rate of adipocyte differentiation/lipogenesis: G3PDH and FAS enzyme activity. Cells were lysed in G3PDH/FAS extraction buffer (0.5% [vol/vol] Triton X-100, 10 mM Tris-HCl, pH 7.5, 20 mM KCl, 1 mM $MgCl_2$, 10% [vol/vol] glycerol, and 0.2 mM dithiothreitol). Cells were collected using an 18-cm cell scraper and incubated on ice for 45 min. Lysates were then centrifuged at $10{,}000 \times g$ for 3 min at 4°C. Supernatants (15 μl for G3PDH activity and 45 μl for FAS activity) were added to reaction buffer (125 mM triethanolamine-HCl, pH 7.5, 2.5 mM EDTA, 0.125 mM β-mercaptoethanol, 0.5 mM NADH, and 1.1 mM dihydroxyacetone phosphate) for G3PDH activity. For FAS activity, supernatants were added to FAS reaction buffer (50 nM KH_2PO_4, 2.5 nM β-mercaptoethanol, 0.25 nM β-NADPH), and 0.1 mM malonyl coenzyme A and acetyl coenzyme A were added to each sample. Absorbance was measured kinetically at 340 nM (20 s) using SkanIt Software 2.4.2 RE for Multiskan Spectrum (Thermo Scientific, Scoresby, Australia). The change in absorbance per minute was used in the formula sourced from Alhaud (2001) to determine enzyme activity (nmol/min/mg) for each sample.

RNA purification and hybridization to microarrays

Microarray analysis was conducted on total cellular RNA collected from cells transfected with Stealth ADAM12 RNAi (ADAM12 RNAi) and Stealth RNAi Negative Control (control) on day 3 ($n = 3$), day 6 ($n = 3$), and day 9 ($n = 3$) posttransfection using the Qiagen RNeasy Mini Kit. Doubled-stranded cDNA was amplified from total cellular RNA (200 ng) using the T7 Primer Promoter from Low Input Quick Amp Labeling Kit (Agilent Technologies). cRNA was then synthesized using T7 RNA polymerase and labeled with cyanine 3-CTP (Low Input Quick Amp Labeling Kit). Amplified cRNAs were purified using Qiagen RNeasy Mini Kit. The amount of cRNA was quantitated using NanoDrop ND-1000 UV-VIS Spectrophotometer (V3.2.1) to determine the specific activity (pmol Cy3 per μg cRNA) for each reaction. Activity greater than six was deemed viable. The quality of cRNA was also assessed using a BioAnalyzer 2100 (Agilent Technologies). Cy3-labeled cRNA (600 ng) was fragmented and incubated at 60°C for exactly 30 min. GEx Hybridization Buffer Hi-RPM was added and centrifuged for 1 mine at 13,000 rpm. Four samples were loaded into an Agilent Microarray SureHyb Hybridization Chamber (Santa Clara, CA). SureHy hybridization chambers were placed into a hybridization oven (Santa Clara, CA) overnight (17 h) at 65°C. Hybridization chambers were removed from hybridization ovens and slides were dissembled and placed in a slide rack immersed in GE wash buffer 1. Slides were then transferred to GE wash buffer 2 at 37°C. Slides were then removed and placed into the scanning cassette of a high-resolution Agilent microarray scanner (Santa Clara, CA).

Microarray analysis

All data analysis was performed using the R (3.3.1) statistical programming language, primarily using the *limma* (3.30.13) Bioconductor (3.4) package (Ritchie *et al.*, 2015). The raw fluorescence signal was background-corrected (Ritchie *et al.*, 2007) and quantile normalized (Bolstad *et al.*, 2003). The 95th percentile of the negative control probes on each array was calculated; only probes ≥10% brighter than the negative controls on at least three arrays were retained for further analysis. The signal from all probes measuring the same gene was averaged, resulting in a single expression value for each gene in each sample. Genes without Entrez IDs were also removed, leaving 14,162 genes for differential expression analysis.

Gene-wise linear models were fitted using *limma* to determine differences in gene expression between treated and control samples, across all three time points and at each individual time point. Empirically estimated array weights, which indicate the relative reliability of each array, were used to down-weight outlying samples (Ritchie *et al.*, 2006). Statistically significant DE genes were identified using empirical Bayes moderated *t* tests (Smyth, 2005), allowing for a mean-variance trend and performing robust empirical Bayes shrinkage of the gene-wise variances to protect against hypervariable genes (Phipson *et al.*, 2016). *p* values were adjusted for false discovery rate using the Benjamini-Hochberg method (Benjamini and Hochberg, 1995).

Overrepresentation of GO terms among significantly DE genes was tested using one-sided hypergeometric tests as implemented in *limma* (Ritchie *et al.*, 2007). The sets of matrisome genes (Naba *et al.*, 2012) extracted from the C2 curated gene sets in the Broad Institute MSigDB were tested for differential expression using the "roast" self-contained gene set testing method (Wu *et al.*, 2010).

All canonical pathways from the C2 curated gene sets in the Broad Institute MSigDB were tested using the "camera" competitive gene set testing method (Wu and Smyth, 2012). "Camera" accounts for intergene correlation while testing whether a set of genes is highly ranked relative to other genes in terms of differential expression.

Quantitative real-time PCR

Reverse transcription and qRT-PCR were done as described (Hunt *et al.*, 2013) on an independent trial to the microarray. Mean normalized gene expression (MNE) was calculated using *Ppai* (peptidylprolyl isomerase A, also known as cyclophilin A) as the housekeeping gene. Oligonucleotide primer sequences can be found in Supplemental Table 1.

Statistical analysis

Statistical analyses used Genstat 16.0 (VSN International Ltd., UK). Student's *t* test (unpaired-two-sample) was used to compare differences between single measures for control and ADAM12 RNAi. Where three or more time points were measured, REML linear mixed models were used to assess differences between ADAM12 RNAi and control and the effect of time. $p < 0.05$ was considered to be statistically significant. Results are presented as mean ± SEM.

ACKNOWLEDGMENTS

We kindly thank Agilent Technologies (Australia) for generously providing the labeling reagents and arrays for the gene expression data presented in this paper. This work was supported by the Cooperative Research Centre for Beef Genetic Technologies, the Department of Primary Industries Victoria, Muscular Dystrophy Australia, the Murdoch Children's Research Institute, and the Victorian Government's Operational Infrastructure Support Program.

REFERENCES

Alhaud G (ed.) (2001). Methods in Molecular Biology: Adipose Tissue Protocols, Totowa, NJ: Humana Press.

Baxter RC, Twigg SM (2009). Actions of IGF binding proteins and related proteins in adipose tissue. Trends Endocrinol Metab 20, 499–505.

Benjamini Y, Hochberg Y (1995). Controlling the false discovery rate: a practical and powerful approach to multiple testing. J R Stat Soc 57, 289–300.

Bodine SC, Stitt TN, Gonzalez M, Kline WO, Stover GL, Bauerlein R, Zlotchenko E, Scrimgeour A, Lawrence JC, Glass DJ, Yancopoulos GD (2001). Akt/mTOR pathway is a crucial regulator of skeletal muscle hypertrophy and can prevent muscle atrophy in vivo. Nat Cell Biol 3, 1014–1019.

Bolstad BM, Irizarry RA, Astrand M, Speed TP (2003). A comparison of normalization methods for high density oligonucleotide array data based on variance and bias. Bioinformatics 19, 185–193.

Brun RP, Tontonoz P, Forman BM, Ellis R, Chen J, Evans RM, Spiegelman BM (1996). Differential activation of adipogenesis by multiple PPAR isoforms. Genes Dev 10, 974–984.

Chan SS, Schedlich LJ, Twigg SM, Baxter RC (2009). Inhibition of adipocyte differentiation by insulin-like growth factor-binding protein-3. Am J Physiol Endocrinol Metab 296, E654–E663.

Clemens MJ, McNurlan MA (1985). Regulation of cell proliferation and differentiation by interferons. Biochem J 226, 345–360.

Davis MR, Arner E, Duffy CR, De Sousa PA, Dahlman I, Arner P, Summers KM (2016). Expression of FBN1 during adipogenesis: relevance to the lipodystrophy phenotype in Marfan syndrome and related conditions. Mol Genet Metab 119, 174–185.

Duffy MJ, Lynn DJ, Lloyd AT, O'Shea CM (2003). The ADAM s family of proteins: from basic studies to potential clinical applications. Thromb Haemost 89, 622–631.

Eto K, Puzon-McLaughlin W, Sheppard D, Sehara-Fujisawa A, Zhang X-P, Takada Y (2000). RGD-independent binding of integrin $\alpha_9\beta_1$ to the ADAM-12 and -15 disintegrin domains mediates cell-cell interaction. J Biol Chem 275, 34922–34930.

Firth SM, Baxter RC (2002). Cellular actions of the insulin-like growth factor binding proteins. Endocr Rev 23, 824–854.

Floyd S, Favre C, Lasorsa FM, Leahy M, Trigiante G, Stroebel P, Marx A, Loughran G, O'Callaghan K, Marobbio CM, *et al.* (2007). The insulin-like growth factor-I–mTOR signaling pathway induces the mitochondrial pyrimidine nucleotide carrier to promote cell growth. Mol Biol Cell 18, 3545–3555.

Fowlkes JL, Enghild JJ, Suzuki K, Nagase H (1994). Matrix metalloproteinases degrade insulin-like growth factor-binding protein-3 in dermal fibroblast cultures. J Biol Chem 269, 25742–25746.

Hertzog PJ, Hwang SY, Kola I (1994). Role of interferons in the regulation of cell proliferation, differentiation, and development. Mol Reprod Dev 39, 226–232.

Hunt LC, Upadhyay A, Jazayeri JA, Tudor EM, White JD (2013). An anti-inflammatory role for leukemia inhibitory factor receptor signaling in regenerating skeletal muscle. Histochem Cell Biol 139, 13–34.

Iba K, Albrechtsen R, Gilpin B, Frohlich C, Loechel F, Zolkiewska A, Ishiguro K, Kojima T, Liu W, Langford K, *et al.* (2000). The cysteine-rich domain of human ADAM 12 supports cell adhesion through syndecans and triggers signaling events that lead to β1 intergrin-dependent cell spreading. J Cell Biol 149, 1143–1155.

Kadowaki T, Yamauchi T (2005). Adiponectin and adiponectin receptors. Endocr Rev 26, 439–451.

Kawaguchi N, Sundberg C, Kveiborg M, Moghadaszadeh B, Asmar M, Dietrich N, Thodeti CK, Moller P, Mercurio AM, Albrechtsen R, Wewer U (2003). ADAM12 induces actin cytoskeleton and extracellular matrix reorganisation during early adipocyte differentiation by regulating β1 integrin function. J Cell Sci 116, 3893–3904.

Kawaguchi N, Xu X, Tajima R, Kronqvist P, Sundberg C, Loechel F, Albrechtsen R, Wewer U (2002). ADAM 12 protease induces adipogenesis in transgenic mice. Am J Pathol 160, 1895–1903.

Krause MP, Liu Y, Vu V, Chan L, Xu A, Riddell MC, Sweeney G, Hawke TJ (2008). Adiponectin is expressed by skeletal muscle fibers and influences muscle phenotype and function. Am J Physiol Cell Physiol 295, C203–C212.

Kurisaki T, Masuda A, Sudo K, Sakagami J, Higashiyama S, Matsuda Y, Nagabukuro A, Tsuji A, Nabeshima Y-I, Asano M, *et al.* (2003). Phenotypic analysisof meltrin α (ADAM12)-deficient mice: involvement of meltrin α in adipogenesis and myogenesis. Mol Cell Biol 23, 55–61.

Kveiborg M, Albrechtsen R, Couchman JR, Wewer UM (2008). Cellular roles of ADAM12 in health and disease. Int J Biochem Cell Biol 40, 1685–1702.

Laplante M, Sabatini DM (2012). mTOR signaling in growth control and disease. Cell 149, 274–293.

Lefterova MI, Lazar MA (2009). New developments in adipogenesis. Trends Endocrinol Metab 20, 107–114.

Loechel F, Fox JW, Murphy G, Albrechtsen R, Wewer UM (2000). ADAM 12-S cleaves IGFBP-3 and IGFBP-5 and is inhibited by TIMP-3. Biochem Biophys Res Commun 278, 511–515.

Loechel F, Gilpin B, Engvall E, Albrechtsen R, Wewer U (1998). Human ADAM 12 (Meltrin α) is an active metalloprotease. J Biol Chem 273, 16993–16997.

Masaki M, Kurisaki T, Shirakawa K, Sehara-Fujisawa A (2005). Role of meltrin α (ADAM12) in obesity induced by high-fat diet. Endocrinology 146, 1752–1763.

McDonough PM, Agustin RM, Ingermanson RS, Loy PA, Buehrer BM, Nicoll JB, Prigozhina NL, Mikic I, Price JH (2009). Quantification of lipid droplets and associated proteins in cellular models of obesity via high-content/high-throughput microscopy and automated image analysis. Assay Drug Dev Technol 7, 440–460.

McLennan SV, Wang XY, Moreno V, Yue DK, Twigg SM (2004). Connective tissue growth factor mediates high glucose effects on matrix degradation through tissue inhibitor of matrix metalloproteinase type 1: implications for diabetic nephropathy. Endocrinology 145, 5646–5655.

Naba A, Clauser KR, Hoersch S, Liu H, Carr SA, Hynes RO (2012). The matrisome: *in silico* definition and *in vivo* characterization by proteomics of normal and tumor extracellular matrices. Mol Cell Proteomics 11, M111.014647.

Page-McCaw A, Ewald AJ, Werb Z (2007). Matrix metalloproteinases and the regulation of tissue remodelling. Nat Rev Mol Cell Biol 8, 221–233.
Phipson B, Lee S, Majewski IJ, Alexander WS, Smyth GK (2016). Robust hyperparameter estimation protects against hypervariable genes and improves power to detect differential expression. Ann Appl Stat 10, 946–963.
Rajkumar K, Modric T, Murphy LJ (1999). Impaired adipogenesis in insulin-like growth factor binding protein-1 transgenic mice. J Endocrinol 162, 457–465.
Ritchie ME, Diyagama D, Neilson J, van Laar R, Dobrovic A, Holloway A, Smyth GK (2006). Empirical array quality weights in the analysis of microarray data. BMC Bioinf 7, 261.
Ritchie ME, Phipson B, Wu D, Hu Y, Law CW, Shi W, Smyth GK (2015). Limma powers differential expression analyses for RNA-sequencing and microarray studies. Nucleic Acids Res 43, e47.
Ritchie ME, Silver J, Oshlack A, Holmes M, Diyagama D, Holloway A, Smyth GK (2007). A comparison of background correction methods for two-colour microarrays. Bioinformatics 23, 2700–2707.
Rommel C, Bodine SC, Clarke BA, Rossman R, Nunez L, Stitt TN, Yancopoulos GD, Glass DJ (2001). Mediation of IGF-1-induced skeletal myotube hypertrophy by PI(3)K/Akt/mTOR and PI(3)K/Akt/GSK3 pathways. Nat Cell Biol 3, 1009–1013.
Rosen BS, Cook KS, Yaglom J, Groves DL, Volanakis JE, Damm D, White T, Spiegelman BM (1989). Adipsin and complement factor D activity: an immune-related defect in obesity. Science 244, 1483–1487.
Roy R, Wewer UM, Zurakowski D, Pories SE, Moses MA (2004). ADAM 12 cleaves extracellular matrix proteins and correlates with cancer status and stage. J Biol Chem 279, 51323–51330.
Ruan W, Lai M (2010). Insulin-like growth factor binding protein: a possible marker for the metabolic syndrome? Acta Diabetol 47, 5–14.
Schlondorff J, Blobel CP (1999). Metalloprotease-disintegrins: modular proteins capable of promoting cell-cell interactions and triggering signals by protein-ectodomain shedding. J Cell Sci 112, 3606–3617.
Shi Z, Xu W, Loechel F, Wewer UM, Murphy LJ (2000). ADAM 12, a disintegrin metalloprotease, interacts with insulin-like growth factor-binding protein-3. J Biol Chem 275, 18574–18580.
Smyth G (2005). Limma: linear models for microarray data. In: Bioinformatics and Computational Biology Solutions Using R and Bioconductor, ed. W. Huber, R. Gentleman, S. Dudoit, V. Carey, and R. Irizarry, New York: Springer-Verlag, 397–420.
Sternlicht MD, Werb Z (2001). How matrix metalloproteinases regulate cell behavior. Annu Rev Cell Dev Biol 17, 463–516.
Streuli C (1999). Extracellular matrix remodelling and cellular differentiation. Curr Opin Cell Biol 11, 634–640.
Tan JT, McLennan SV, Song WW, Lo LW, Bonner JG, Williams PF, Twigg SM (2008). Connective tissue growth factor inhibits adipocyte differentiation. Am J Physiol Cell Physiol 295, C740–C751.
Wewer UM, Morgelin M, Holck P, Jacobsen J, Lydolph MC, Johnsen AH, Kveiborg M, Albrechtsen R (2006). ADAM12 is a four-leafed clover: the excised prodomain remains bound to the mature enzyme. J Biol Chem 281, 9418–9422.
Wu D, Lim E, Vaillant F, Asselin-Labat ML, Visvader JE, Smyth GK (2010). ROAST: rotation gene set tests for complex microarray experiments. Bioinformatics 26, 2176–2182.
Wu D, Smyth GK (2012). Camera: a competitive gene set test accounting for inter-gene correlation. Nucleic Acids Res 40, e133.
Zappala G, Rechler MM (2009). IGFBP-3, hypoxia and TNF-α inhibit adiponectin transcription. Biochem Biophys Res Commun 382, 785–789.
Zhou Z, Darwal MA, Cheng EA, Taylor SR, Duan E, Harding PA (2013). Cellular reprogramming into a brown adipose tissue-like phenotype by co-expression of HB-EGF and ADAM 12S. Growth Factors 31, 185–198.
Zolkiewska A (1999). Disintegrin-like/cysteine-rich region of ADAM 12 is an active cell adhesion domain. Exp Cell Res 252, 423–431.